-85-1706

CONF-8503137--4

RECEIVED BY OSTI JUN 07 1985

LA-UR--85-1706

DE85 012713

TITLE: REVIEW OF THE LOS ALAMOS FRX-C EXPERIMENT

AUTHOR(S): R. E. Siemon, W. T. Armstrong, D. C. Barnes,*R. R. Bartsch, R. E. Chrien, J. C. Cochrane, W. Hugrass, R. W. Kewish, P.L. Klingner, H. R. Lewis, R. K. Linford, K. F. McKenna, R. D. Milroy,** D. J. Rej, J. L. Schwarzmeier, C. E. Seyler,*** E. G. Sherwood, R. L. Spencer,**** and M. Tuszewski

SUBMITTED TO: Proc. of IAEA Technical Committee Meeting on Advances in Compact Toroid Research, Sidney, Australia, March 4-6, 1985. In care of: Prof. I. Jones, The Flinders University of South Australia, School of Physical Sciences, Bedford Park, South Australia 5042 Australia

*Present address: Science Applications, Inc., Austin, Texas
**Present address: Spectra Technologies, Bellevue, Washington
***Present address: Cornell University, Ithaca, New York
****Present addr[illegible] Brigham Young University, Provo, Utah

MASTER

Los Alamos Los Alamos National Laboratory
Los Alamos, New Mexico 87545

Review of the Los Alamos FRX-C Experiment

Richard E. Siemon, W. Thomas Armstrong, R. Richard Bartsch, Robert E. Chrien, James C. Cochrane, Waheed N. Hugrass, Ralph W. Kewish, Jr., Phillip L. Klingner, H. Ralph Lewis, Rulon K. Linford, Kenneth F. McKenna, Donald J. Rej, James L. Schwarzmeier, Eugene G. Sherwood, and Michel Tuszewski

Los Alamos National Laboratory
Los Alamos, NM 87545

Daniel C. Barnes

Science Applications International Corporation,
1406 Camp Craft Rd. Suite 202A, Austin, TX 78746

Richard D. Milroy

Spectra Technologies, Inc.
2755 Northup Way, Bellevue, WA 98004

Charles E. Seyler

Cornell University,
215 Phillips Hall, Ithaca, NY 14853

Ross L. Spencer

Brigham Young University,
296 ESC, Provo, UT 84602

Presented by A. R. Sherwood

Abstract

The FRX-C device is a large field-reversed theta pinch experiment, with linear dimensions twice those of its FRX-A and FRX-B predecessors. It is used to form field-reversed configurations (FRCs), which are high-beta, highly prolate compact toroids. FRX-C has demonstrated an R^2 scaling for particle confinement in FRCs, indicating particles are lost by diffusive processes. Particle losses were also observed to dominate the energy balance. FRC lifetimes exceeding 300 μs were observed when weak quadrupole fields were applied to stabilize the $n = 2$ rotational mode. Detailed studies of the FRC equilibrium were performed using multi-chord and holographic interferometry. Measurements of electron temperature by Thomson scattering showed a flat profile and substantial losses through the electron channel. The loss rate of the internal poloidal flux of the FRC was observed to be anomalous and to scale less strongly with temperature than predicted from classical resistivity.

Following a modification to the device, FRCs were translated from the theta-pinch coil into a dc solenoid and metallic vacuum chamber. The translation process was observed to be in reasonable agreement with adiabatic theory. FRCs were translated and trapped in a dc solenoid without active auxiliary coils. Trapping was aided by the inelastic reflection of FRCs off a magnetic mirror. Measurements of the radiated power from translating FRCs indicated that radiation is a small component in the power balance and thus it appears that electron thermal conduction is more important.

The particle confinement of an FRC is expected to improve as $\bar{s}$, which measures the number of local ion gyroradii between the field null and the separatrix, increases. However, a regime of increased susceptibility to MHD modes, notably the internal tilt, has recently been predicted to have a threshold in $\bar{s}$ of three to four. To address these issues, as well as the issues of electron energy loss and poloidal flux loss, a three-stage experiment has been proposed which is predicted to reach $\bar{s}$ of about 7. The FRX-D device will consist of separate formation, heating, and confinement regions. Plasma translation permits separation of these functions in a manner thought to be desirable for a fusion reactor.

I. Background

The Field-Reversed Configuration (FRC). The FRC is a type of compact toroid that is formed with purely poloidal magnetic fields. As shown in Fig. 1, it is a toroidal magnetic configuration in which closed poloidal field lines surround a field null. A magnetic separatrix located at radius r_s separates a region of closed lines that displays relatively good plasma confinement from a region of open lines that displays relatively poor plasma confinement. In the FRC experiments described in this paper, the configuration was formed using a field-reversed theta pinch. In these experiments the plasma was confined in a separatrix volume that was prolate and elongated as shown in Fig. 1.

Particular features of the FRC that offer advantages in application to a fusion reactor are the following.

- The plasma beta is the highest known for any fusion oriented magnetic configuration. This implies efficient use of magnetic field energy in a reactor and high power density using magnets with modest field strength.
- The geometry of the external coils (and blanket) is cylindrical, which lends itself to modular systems and ease of engineering.
- The field line structure results in a natural divertor that deposits exhaust plasma conveniently at the ends of a cylindrical system.
- The FRC plasma is readily translated as a self-contained structure from one coil to another by means of a weak gradient in a solenoidal guide field. This permits separating the functions of formation, heating, and nuclear burn.

The engineering simplifications achieved by this separation of functions and linear arrangement offers the potential for an economical reactor with small unit power and high power density, conceivably using special features such as a liquid metal first wall. Small unit power is possible because the total reactor volume,[1] even in a multistage linear system, is projected to be much less than in tokamak reactor designs such as the STARFIRE.[2] Such projections are, however, dependent upon FRC confinement physics, and their evaluation will require confinement scaling studies in a regime of parameters closer to reactor-like conditions.

Equilibrium. For an elongated equilibrium in a cylindrical coil, the volume averaged pressure within the separatrix relative to the external magnetic field pressure, $\langle\beta\rangle$, is given by the simple formula first derived by D. C. Barnes:[3,4]

$$\langle\beta\rangle = 1 - x_s^2/2, \qquad (1)$$

where x_s is the ratio of the separatrix radius to the coil radius (see Fig. 1). This result, independent of the pressure profile, is required by axial force balance. In the radial direction magnetic field pressure balances plasma pressure, and in the axial direction field line tension balances the pressure. The average beta formula requires corrections when one takes into account finite orbit effects, finite elongation (field-line curvature in the midplane), or magnetic mirrors (nonuniform coil in the axial direction).[5] Nevertheless, the formula is a reasonable approximation in many instances, and it has provided a great deal of insight into FRC phenomena. Many useful analytic estimates are facilitated by Eq. (1). A corollary of this result is that the poloidal flux contained in the FRC is bounded by two pressure profiles that represent extrema with respect to possible pressure profiles.[6] This is seen, for example, in the response of the plasma to adiabatic compression.[7]

Results from FRX-A and FRX-B. Following the report of interesting results in the Soviet Union[8] and Germany[9] in the early 70s, a series of experiments was started at Los Alamos by R. K. Linford in 1976. Typical parameters achieved in these early Los Alamos experiments[3] are summarized in Table I and typical magnetic field waveforms are shown in Fig. 2. Although the plasma lifetimes observed were limited to a maximum value of less than 100 μs, the lifetimes were considerably greater than the characteristic Alfvén transit times (1 → 10 μs). This result is in disagreement with MHD model predictions of an internal tilt instability, which is predicted to have a characteristic growth time of an Alfvén transit time around the longest closed field line.[10] Recent calculations based on a kinetic plasma model (see Section XI.) appear to resolve this paradox as discussed in the last section of this paper.

Rotation vs. Particle Loss. The issue that emerged as a result of the experiments on FRX-A and FRX-B was the following. Given that the FRC can be formed in a high-beta equilibrium that appears experimentally to be MHD stable, what fundamental limitations would prevent increasing the confinement time to the Lawson condition? The most obvious problem observed in experiments was that the plasma lifetime was limited by a rotationally driven n = 2 fluting mode. The mode represents an elliptical distortion that grows so large that the FRC contacts the vacuum chamber and then rapidly decays. Following a quiescent period, the mode is observed to grow as the bulk rotational frequency approaches

the ion diamagnetic frequency.[11] During the quiescent period, one also observes that particles diffuse across the closed field lines until they reach the separatrix where they rapidly leave at the thermal speed along the open field lines. Plasma rotation can be caused by ions with angular momentum antiparallel to the external field being lost more rapidly than ions with the opposite sign of angular momentum[12] and this rotation can be enhanced by end-shorting of the open field line plasma.[13,14] Therefore, the fundamental limitation for FRCs is particle diffusion and not the rotational mode, and attention should be focused on the cause of particle diffusion.

This view influenced the proposal of FRX-C in 1979[15] and the early portion of the experimental program. The purpose of FRX-C was to test the particle confinement in a regime of increased size relative to an ion gyroradius while approaching a more MHD-like regime where the possibility of tilt instability would be greater. Qualitatively the issues facing the FRC program today are similar, but the quantitative understanding of these issues has improved markedly. Also, equally important issues have emerged concerning the decay rate of poloidal flux and electron thermal conduction. The rotational mode has somewhat subsided as an issue, because numerous experiments have since demonstrated that the rotational mode can be suppressed by the addition of weak multipole fields.[16-19] As an example, quadrupole stabilization on the FRX-C device is reported here in Sec. V.

II. Experimental Method

Description of Device. The FRX-C theta pinch has a dual-fed, 50-cm-diameter, 200-cm-long coil. The system is shown schematically in Fig. 3 and has been described elsewhere.[20,21] A number of the electrical and mechanical parameters are listed in Table II. It is presently the largest field-reversed theta pinch in operation and has accordingly displayed the longest FRC lifetimes.

High and Low Fill Pressure Operation. The gas pressure of deuterium when the discharge is initiated is a convenient parameter used to adjust several important characteristics of the FRC. At low initial fill pressure, the radial implosion is more rapid and the resulting ion temperature is higher. At high initial fill pressure, the temperature is lower, the final density is higher, and because the magnetic field is only weakly dependent on initial pressure (mainly because of adjustments in the initial bias field), the high pressure

operation results in the maximum ratio of plasma size to ion gyroradius, which is found to correspond to the longest plasma confinement time. In most of the data presented in this paper, a comparison is made between results obtained at initial pressures of 5 and 20 mtorr. These fill pressures along with associated adjustments in preionization conditions and bias field represent standard operating conditions under which most diagnostic data runs such as holographic interferometry and Thomson scattering were conducted. Representative plasma parameters at the beginning of the quiescent phase are listed in Table III together with the characteristic confinement times.

The two pressures 5 and 20 mtorr also represent approximate boundaries of operation possible for the FRX-C experiment. At lower pressure the two available methods of preionization (PI) both become marginal (ϑ-pinch discharge as seen in Fig. 2, and Z discharge). At higher pressure the main problem is that the FRC equilibrium is too long to fit within the length of the theta-pinch coil. The formation process results in an FRC with increasing length as a function of fill pressure.[22] Above 20 mtorr the ends of the FRC expand into the vacuum beyond the coil allowing the plasma to escape. Also, at higher pressure the temperature drops below 100 eV and there is concern that the phenomena might be unduly influenced by collisionality or impurity radiation.

FRX-C/T Modification. Apart from minor modifications such as the addition of quadrupole current conductors for stabilization of the rotational n = 2 mode, the FRX-C experiment was operated as shown in Fig. 3 from August 1981 until the summer of 1983. At that time a major modification was installed:[23] a dc solenoid and 6-m-long vacuum chamber were placed at the end of the FRX-C coil to permit studies of the translation process. A photograph of the modified facility, which was renamed FRX-C/T, is shown in Fig. 4. The experimental results are discussed below in Sec. IX.

III. FRC Equilibria

Experimental Studies. The high-beta nature of FRC equilibria has been the subject of detailed studies in FRX-B and FRX-C. In FRX-B, radial pressure balance between plasma pressure at the field null and the external magnetic pressure has been verified through independent measurements of electron and ion temperatures, density, and magnetic field[3]. In FRX-C, the existence of an FRC equilibrium was also evident from holographic interferograms (see Section IV.)

which showed a sharp density gradient at the separatrix persisting throughout the FRC lifetime.[19]

Radial and axial profiles of the line-integral density $\int ndl$ have been obtained in FRX-C.[24] The radial $\int ndl$ profile (Fig. 5) was inconsistent with flat or parabolic density profiles within the separatrix radius, but was in good agreement with the type of profile expected for an FRC equilibrium. The radial profile was peaked for finite radius of tangency d ($d/r_s \approx 0.3$) because of the density depression near the geometric axis of an FRC. The height of the peak provided an estimate of the separatrix density n_s which was found to be 50-60% of the maximum density n_M at the field null. The average density inferred from the radial profile was $(0.90\pm0.05)n_M$ which, together with the observation of flat temperature within the separatrix[3,25] and radial pressure balance, was consistent with the value of $\langle\beta\rangle$ predicted by Eqn. 1.

Radial $\int ndl$ data[24] during the growth of the n=2 rotational mode also provided an estimate of the characteristic density gradient scale length $\ell_n(r_s)$ at the separatrix. The quantity w, defined as $\ell_n(r_s)/\rho_{i0}$, was found to be 4-5, in agreement with the data found from end-on holographic interferograms[26] and similar to that of another rotational analysis[18] (here, $\rho_{i0} \equiv (k_B T_i m_i^{-1})^{1/2}\Omega_i^{-1}$ is the ion gyroradius evaluated using the external ion gyrofrequency Ω_i and the average ion temperature, k_B is Boltzmann's constant, and m_i is the ion mass).

The axial profile of $\int ndl$ was found to be approximately elliptical in shape[24] (Fig. 6). The $\int ndl$ and excluded flux radius[27] $r_{\Delta\varphi}$ profiles were similar, implying that the line-averaged density was fairly constant along the FRC length. Measurements of the dynamic features of the FRC were seen to correlate in detail between the two diagnostics.

Computation of Equilibria. The computation of FRC equilibria within the MHD model has proven to be surprisingly difficult.[28] In order to match the axial variation of $\int ndl$ observed in FRX-C (Fig. 6), it is necessary to compute equilibria with internal flux surfaces that are elliptical in shape and which are distributed gradually in the axial direction.[5] This type of equilibrium appears to be the preferred output of a code[29] using an entropy-like variable in a $1\frac{1}{2}$-D formulation of the equilibrium problem. In this case specifying a smooth entropy-like variable (as a function of flux) gives rise to a pressure gradient which is sharply peaked at the separatrix. However, in a code[28] in which the pressure profile (as a function of flux) is specified smoothly, the preferred output is more racetrack in shape. The latter code can also find elliptical

equilibria if the pressure gradient is sufficiently peaked at the separatrix.[5] It is not understood why the codes tend to generate different equilibria, and it is not known why or even if such steep pressure gradients at the separatrix are required to produce equilibria that match the experimental data.

IV. Particle Confinement

Measured Inventory Decays Rapidly. The rate at which particles diffuse out of the closed-field line region of the FRC appears to be the dominant loss process in the FRX-C experiment. The loss rate is approximately ten times faster than classical even when the pronounced density gradients associated with the high-beta equilibrium of the FRC are taken into account.[30] The loss rate is determined by measuring the total inventory of particles as a function of time during the quiescent phase. It is assumed that no significant source of particles exists within the separatrix. This assumption is supported by plasma particle inventory measurements which account for $\geq$ 80 % of the fill gas within the coil length during formation.[26] Further support is obtained from calculations[31] that show that the deuterium influx level is small. In addition, any ionization of this influx occurs almost entirely on the open field lines. The plasma on these field lines is diverted toward the end of the vacuum vessel.

Methods of Measurement. Two complementary methods of interferometry have been used to determine the particle inventory as a function of time.[26] In the side-on method a 3.39-micron laser measures the line-integrated density along a path perpendicular to the cylindrical axis. Diamagnetism of the FRC is measured by means of a magnetic probe array along the coil.[27,32] The separatrix volume determined by the probe array, and the density determined as a function of time by the interferometer provide enough information to estimate the particle inventory as a function of time given the high-beta equilibrium model for the FRC.

In the end-on method a holographic interferogram is formed during a 30 ns interval at one time during each discharge. A typical interferogram is shown in Fig. 7. The fringe shift relative to the straight background fringe pattern is a measure of the line-integrated electron density at each position in the interferogram. The area integral of the fringe shift thus yields the total electron inventory in the field of view. The density profile deduced from the interferogram is found to be azimuthally symmetric. Except for corrections that are needed to account for the exhaust plasma,[33] the holographic method provides

the most accurate measurement of electron inventory because it is insensitive to axial dynamics, multiple field nulls, changing density profiles, sideways shifts, and other effects which can cause errors in the side-on method.

Confinement Scales as R^2. The measurements of τ_N obtained on FRX-C are summarized in Fig. 8. The confinement times are plotted vs. R^2/ρ_{io} where R is the radius of the magnetic field null ($r_s/\sqrt{2}$). This scaling as discussed below is suggested by theoretical models for particle confinement that use a lower-hybrid-drift (LHD)[34] form of resistivity. The holographic interferometer determinations were done at 5 and 20 mtorr using the data shown in Fig. 9. After correction for the exhaust plasma,[33] the confinement time at 20 mtorr was 154 ± 25 μs. These data correspond to the points at R^2/ρ_{io} equal to about 90 cm and 240 cm, respectively. The FRX-B point was obtained with the side-on method using data combined from several experimental runs.[3] The FRX-B experiments at 17 mtorr provided similar plasma parameters (density, temperature, magnetic field, ρ_{io}, and x_s) as in the FRX-C 20 mtorr data. The comparison of FRX-B at 17 mtorr and FRX-C at 20 mtorr provides strong evidence that confinement scales approximately as the square of radius in the present experimental regime. An increase in τ_N from 39 to 154 μs resulting from an increase in R by a factor of two is characteristic of diffusive losses out of a toroidal configuration and implies that gross magnetohydrodynamic instabilities are not dominating the loss process.

Comparison with LHD models. The variation of confinement for fixed size and x_s is predicted by LHD models to be approximately a $1/\rho_{io}$ dependence.[30] The data in Fig. 8 support this prediction in that FRX-C data points obtained with various operating parameters have similar plasma radii but different ion gyroradii, and the points tend to follow the R^2/ρ_{io} scaling. The intermediate FRX-C points were obtained using 5 mtorr with reduced magnetic field, and the side-on method of interferometry. The 5-mtorr full-field point (τ_N = 67 ± 25 μs), which corresponds to the largest ion gyroradius, was obtained with the end-on holographic interferometry method (Fig. 9). Insufficient data on the exhaust plasma at 5 mtorr conditions was available to permit correction of this point. The side-on method gave a somewhat larger value ($\tau_N \approx 100$ μs). For both methods the uncertainty in the analysis was increased for this condition because the period of observation was limited by the relatively early onset of the n = 2 rotation.

Additional confinement scaling data have been obtained in the modified FRX-C/T[35] and in the TRX experiment at Spectra Technology[36] using the side-on method. In these experiments, the predictions of LHD seem to depart somewhat from experimental trends, although the magnitude of the LHD prediction is usually within a factor of 2. The temperature dependence in particular appears to be more favorable as determined empirically than is given by the $1/\rho_{io}$ dependence of LHD. Thus additional experiments are needed to determine the scaling of particle confinement with temperature.

In summary, the LHD model provides a better estimate of particle confinement in FRCs than any other theoretical model so far developed. Attempts to measure LHD turbulence by means such as collective light scattering are presently in progress at Osaka University and the University of Washington. Some experimental data indicate scaling laws which differ from the predictions of LHD. Thus the understanding of particle confinement in FRCs is far from complete and much more work is needed in this important area.

V. Quadrupole Stabilization

Experimental Demonstration. It was reported by the FRC group at Osaka University[16,17] that the application of relatively weak quadrupole fields, applied during the quiescent phase after the FRC is formed, results in a grossly stable FRC with no rotational $n = 2$ mode. The group at Spectra Technology reported a similar effect using octupole fields.[18] Data are reported here that show the stabilizing effect of quadrupoles on the FRX-C experiment.[19]

FRX-C Data. The quadrupole field waveform was similar to that of the main field with a risetime of 5 μs and a crowbarred decay time of 350 μs. Its magnitude was adjusted by varying the voltage on the quadrupole capacitors and the time at which the quadrupole current was crowbarred.

In initial experiments, irreproducible FRC formation and stabilization was associated with current induced in the quadrupole coils by the theta-pinch current. The quadrupole circuit was modified to reduce the induced current, and thereafter reproducible FRCs could be formed and stabilized. The stabilization is illustrated (Fig. 10) by end-viewing holographic interferograms. The severe $n = 2$ distortion was completely suppressed and the FRC shape assumed four-fold symmetry when the quadrupole fields were applied. However, the FRC showed a tendency to shift when the quadrupole fields were applied. Data from the holographic interferograms indicated that the FRC tended to shift vertically

toward the collector plate feedslots by 2.1 ± 1.9 cm, possibly because of asymmetries in the quadrupole fields.

The stabilization was insensitive to the time of quadrupole field initiation over the range -2 μs to 40 μs relative to the main bank time. The threshold field required for stabilization was observed to be 15 → 25% of the threshold predicted by the MHD model of Ishimura.[37] The time histories of the main field, plasma separatrix radius, separatrix length, average density, and pressure-balance temperature are shown in Fig. 11 for 20 mtorr fill pressure. Without quadrupoles, the FRC stable period was about 100 μs. With quadrupole fields the plasma lifetime was extended to over 300 μs (comparable to the decay time of the magnetic field). Similar stabilization results were obtained at 5 mtorr fill pressure as shown in Fig. 12. The decay times of the particle inventory, energy, and internal flux were similar in both the stabilized and unstabilized FRCs for each fill pressure case.

The effect of quadrupole fields on plasma fluid rotation was studied by observing the doppler shift of CV emission (227.1 nm). The CV doppler shift was observed using a six channel polychromator with channel spacing and resolution of 0.01 nm which viewed the FRC through a chord tangent to the radius (7 cm) of the field null. In order to obtain adequate CV intensity, it was necessary to reduce the magnetic field to 6 kG and to increase the carbon-to-deuterium concentration to 0.03 by adding methane to the fill gas. The parameter $\alpha \equiv -\Omega/\Omega_i^*$, where Ω is C^{+4} rotational frequency and Ω_i^* is the deuterium diamagnetic frequency calculated using a rigid rotor model,[3] are shown in Fig. 13 for the same discharges illustrated in Fig. 12. In the absence of quadrupole fields, α increased during the stable period but began to decrease when the n = 2 mode neared its maximum deformation. When the quadrupole fields were applied, α fluctuated about zero throughout the FRC lifetime. This result differs from reports of a persistent rotating deformation in partially stabilized FRCs [16,18] and the absence of variation in the measured CV doppler shift in another experiment[38]. This difference remains to be resolved.

Helical Quadrupoles. Following the demonstrations of multipole stabilization of the n = 2 mode, an interesting experiment was reported from Nihon University.[38,39] The multipoles were twisted to form a helical structure and the magnitude of current needed for stabilization was found to be reduced. It has also been noted that whereas straight quadrupoles tend to destroy flux surfaces as the external fields penetrate the FRC structure, helical quadrupoles

have the potential of providing nested flux surfaces even on a long time scale where the fields penetrate into the (possibly) spinning FRC field structure.[40] An experiment planned for FRX-C/T will investigate the use of stabilizing helical quadrupole fields in the translation chamber where the plasma is trapped in dc fields.

Theory. The rotational instability in the presence of multipole fields has been studied with a 2-D hybrid code[41] and by means of the MHD model.[37,42] Both models predict a threshold for stability of the n = 2 mode as the quadrupole field strength is increased. It is difficult to compare the two calculations because the models upon which they are based are quite different, but when their results are applied to specific experiments, the hybrid code threshold is smaller than the MHD threshold by about a factor of two. The MHD threshold is computed assuming that the plasma is circular and that the n = 4 modulation of the quadrupole magnetic pressure can be neglected.[37] Both of these assumptions are unrealistic. Relaxing the second one, while retaining the first one, gives the result that there is no stabilization threshold for the quadrupole case.[37] (The threshold is unchanged for hexapoles, octupoles, etc..[37]) When the first assumption is relaxed, it can be shown that the ideal MHD equilibrium is cusp-shaped,[42] in rough agreement with experiments and with the hybrid simulation.[41] Stability is much harder to analyze for the cusp-shaped equilibrium, but simple estimates indicate that stability is obtained and that the threshold might even be lower then the one predicted in Ref. 37 using a circular plasma and no n = 4 variation in the quadrupole magnetic pressure. This might bring the MHD calculation and the hybrid simulation into agreement. It should be noted, however, that the experiments consistently show thresholds that are factors of two or more below the hybrid simulation threshold.

VI. Energy Confinement

Zero-Dimensional Models. As the first step in investigating the characteristics of energy confinement in FRCs, the plasma can be treated as an elongated equilibrium with separate electrons and ion temperatures but with no radial variations (as observed experimentally[3,25]). Compressional work in such models is estimated using formulas like those of Sec. VIII, and other processes such as thermal conduction, radiation, and ohmic heating are treated as perturbations on the adiabatic assumption.[43-45] More realistic models are under

development,[46-49] but at the present time, our understanding of energy confinement in FRCs is based on the zero-dimensional approach.

FRX-C Results. The time histories of a number of experimentally measured quantities for the standard 20-mtorr conditions are shown in Fig. 14. Similar quantities for the 5-mtorr conditions are shown in Fig. 15. Table IV lists definitions of the various quantities, and how they are measured experimentally. Also shown on these figures are dashed lines representing the results of zero-dimensional modeling in which the values of various confinement times are determined by specific transport models described in Ref. 43. An example of electron temperature measured as a function of radius with Thomson scattering[25] is shown in Fig. 16. Each point was obtained on a separate discharge. Also shown in Fig. 16 is the result of a one-dimensional energy transport calculation including IHD and microtearing transport.[49] In addition to these data, calorimeter measurements of radiated power[35,50,51] were made on full field 5 mtorr translated FRCs but without measurements of the electron temperature. The calorimeter measurements indicated that the radiated power fraction was about 10% of the total power loss from the plasma, which was about 200 MW.

Discussion. Based on these results and the arguments presented in the references cited, the following points have been deduced with regard to energy confinement.

- The $n\tau_E$ product for 20 mtorr is 4×10^{11} $cm^{-3}s$ at T_i = 100 eV and the $n\tau_E$ product for 5 mTorr is 7×10^{10} $cm^{-3}s$ at T_i = 600 eV.
- The major loss of energy is by means of particle transport.
- The second most important channel appears to be anomalous electron thermal conduction.
- Impurities do not appear to radiate enough energy to influence the overall power balance.

The global energy confinement time τ_E, the fraction of losses that are due to particle transport, and the relative magnitude of electron thermal conduction are inferences that depend to some extent upon the assumptions of the zero-dimensional model. The interpretation of radiated power is only weakly dependent on model assumptions, but the measurements are available for relatively few operating conditions and were not done simultaneously with Thomson scattering. In general, our understanding with regard to energy confinement of FRCs is less developed than our understanding of particle

confinement, and again it must be emphasized that a great deal more work is needed on the subject.

VII. Flux Loss

Unknown Mechanism. For FRCs in equilibrium, loss of internal poloidal flux is thought to occur by resistive annihilation at a single field null. The characteristic flux loss time scale τ_φ is difficult to measure experimentally because the flux depends on the magnetic field profile within the separatrix. Therefore, τ_φ is commonly inferred[6,52] from FRC equilibrium models that link φ to external measurements of r_s and B. The values of τ_φ obtained in most experiments correspond to values of resistivity at the field null, $\eta(R)$, that exceed Spitzer transverse resistivity by factors of 3 → 10, assuming a rigid rotor profile. It is unlikely that these anomalies can be explained by impurities.[25,35,50,51] Futhermore, present models for LHD resistivity predict a negligible contribution to $\eta(R)$. Thus the physics of flux loss is unknown at the present time.

Empirical Scaling. Recently empirical scaling laws for τ_φ have been obtained from FRX-C/T[53] and also from TRX-1.[36] These scaling laws and the classical scaling based on Spitzer resistivity are given in Table V. Note that the classical flux loss depends on T_e, whereas the empirical scalings use the pressure balance temperature $T_i + T_e$ which weakens the comparison of the classical and empirical scalings. The most significant departures from classical scaling were the weak scaling with temperature and the inverse scaling with length.

Further evidence of non-classical τ_φ scaling was obtained from comparison of 5 and 20 mtorr fill pressure cases in FRX-C where Thomson scattering determination of T_e was available. This data comparison again indicated a flux loss scaling with temperature ($\tau_\varphi \propto T_e^{0.6 \pm 0.2}$) which was weaker than the classical scaling. It was also noted in FRX-C that departures from the optimum formation conditions (PI timing and PI and bias field amplitudes) resulted in decreases in τ_φ by factors of 1/2 to 1/3.

VIII. Adiabatic Compression

Theory. The response of a high-beta FRC equilibrium to changes in the external magnetic field can be determined approximately by analytic formulas based on the MHD model for elongated equilibria.[7] The change in field can occur

as a result of either changing the flux in a coil of fixed dimension (flux compression), or as a result of changing the radius of the coil (r_w) with a fixed amount of flux (wall compression). In the case of flux compression the value of x_s can be taken as the independent variable. For wall compression, the plasma response is independent of the pressure profile, but for flux compression the response of the plasma is dependent to some extent on the pressure profile. The results of the theory for adiabatic compression are summarized in Table VI, where a parameter ε (defined in Ref. 7) is introduced to represent the variations possible resulting from various diffuse profiles. The value of ε varies from -1, for the extreme profile representing the minimum possible flux, to zero for the other extreme representing the maximum possible flux. Typically in present experiments, the value of ε that corresponds to the observed profiles is about -1/4. As discussed in Sec. IX, these formulas have been found to predict reasonably well the FRC expansion during translation, which results from a change in both wall radius and external flux. The formulas have also been used to predict plasma heating in the proposed FRX-D device described in Sec X.

Experiment. The magnetic field in FRX-C is limited by the size of the available capacitor bank. Therefore, it was not possible to test the predictions of adiabatic compression over a significant range of magnetic field values. However, in the case of full-field 5 mtorr operation, the FRC length tended to be significantly shorter than the coil length, and so it was possible to investigate the adiabatic (flux compression) response of the plasma over a limited range of field values by reducing the final magnetic field. The minimum possible field was determined by the value that resulted in an FRC which expanded beyond the ends of the 2 m coil. In Fig. 17 the results of adiabatic decompression are plotted as a function of final field strength. The formation conditions of preionization, bank voltage, and bias field were held constant, while the final field was adjusted by disconnecting part of the capacitor bank. The adiabatic formulas for the two extreme profiles are also plotted with the experimental data points, and the theory is seen to be in reasonable agreement with the experiment.

IX. Translation

Description of Experiment. In the summer of 1983, the FRX-C experiment was modified to permit study of the translation process.[23,35,54] Other translation experiments have also been reported.[3,39,55,56] As shown in Fig. 18, the

theta-pinch coil was modified to provide a small gradient in the magnetic field. The coil was effectively a conical theta pinch with a cone angle of 1.4 degrees. After the FRC was formed it moved under the influence of a net axial force, which translated the FRC into an adjacent flux conserver and dc solenoid.

Dynamics of Translation. Plotted in Fig. 19 is the time evolution of the excluded flux radius profile $r_{\Delta\varphi}(z)$. The FRC was formed within 10 μs after initiation of the main theta-pinch capacitor bank. Because of inertia, it took approximately another 20 μs for the plasma to be ejected out of the source. The plasma entered the translation region with negligible flux and particle losses and propagated 6 m at maximum speed $v_z \approx 17$ cm/μs before it reflected from the downstream mirror. The speed of the FRC was observed to be less ($v_z \approx 12$ cm/μs) following reflection. The lost translational kinetic energy was observed to be rethermalized into the plasma when the mirror ratio was strongest ($R_M = 5.3$) but could not be accounted for when the mirror ratio was weaker. Particle, thermal energy, and flux losses appeared to be unaffected by the reflection. The FRC translated back towards the source and underwent another reflection from the mirror formed by the crowbarred theta-pinch coil. The plasma eventually settled down near the center of the translation region and it ultimately decayed away after 200 μs. The onset of the $n = 2$ rotational mode occurred later and the mode grew more slowly during these translation experiments.

An important independent variable of the experiment was the strength of the vacuum dc guide field B_o in the translation region. By reducing the guide field the plasma was observed to expand, cool, and accelerate. Plotted in Fig. 20 are the maximum plasma density n_M and pressure balance temperature, $T = T_e + T_i$, observed during the first transit through the translation region. These data are normalized to their respective values in the source and they are plotted against the ratio of the magnitude of the external confining field, $B_w = B_o/(1-x_s^2)$. These data are compared with the predictions of the adiabatic theory[7] (dashed lines). The experimental scalings of n and T with B_w were similar to that of theory; however, the plasma cooled somewhat less in the experiment. For an elongated equilibrium one can show[57] that the total magnetic and plasma energy in a flux conserving region is

$$E_{total} = \frac{1}{2} N m_i v_z^2 + \frac{5}{2} N k_B T + E_{BV} \quad , \qquad (2)$$

where N is the particle inventory inside the FRC separatrix volume and E_{BV} is the total magnetic energy in the region in the absence of plasma. Assuming that E_{BV} is constant in each region and ignoring losses, it follows that the translation speed for an FRC initially at rest can be expressed by the relationship:

$$v_z = \left[\frac{5k_B\Delta T}{m_i}\right]^{1/2} , \qquad (3)$$

where ΔT is the change in the plasma temperature resulting from adiabatic expansion.

As seen from the v_z data in Fig. 21, FRCs moved faster when translated into weaker guide fields. The expected values of v_z given from Eq. (3) and adiabatic theory are shown by the dashed curve. Reasonably good agreement between theory and experiment was obtained for larger B_o; however, at smaller B_o, v_z appeared limited to approximately the ion thermal speed and it was about 25% smaller than that predicted.

Numerical Modeling. FRC translation in FRX-C/T has been numerically modeled using a 2-D MHD code.[58] The simulation shown in Fig. 22 has been computed for 5 mtorr puff, B_o = 2.5 kG, and mirror ratio R_M = 2.5 conditions. Axial asymmetries in magnetic reconnection during formation result in a brief acceleration towards the upstream. The FRC is eventually accelerated downstream to peak speeds, $v_z \approx 19$ cm/μs, over a time scale comparable to that observed experimentally. At the time of the reflection the plasma density is strongly peaked at the downstream end to values 2 to 3 times larger than the average density. Following the reflection the code predicts a speed $v_z \approx 14$ cm/μs, which is similar to the experimental observation that upon reflection the translation speed is reduced by about 30%.

Toroidal Field. Internal magnetic probing measurements of translating FRCs revealed the presence of a toroidal field component.[35,59,60] The B_ϑ component showed a non-reproducible fluctuating structure with peak amplitude of 1/3 → 1/2 of the external field and a volume-averaged rms value of $(0.16 \pm 0.08)B_w$. This range represented toroidal field energy which was 1 → 7 % of the plasma energy and 3 → 30 % of the internal poloidal field energy. The net toroidal flux was typically four times the poloidal flux of the FRC (this magnitude in part

represents a geometrical effect of the elongated FRC). The sense of the toroidal flux was almost always left-handed with respect to the direction of translation out of the theta pinch coil, suggesting a connection with the translation process.

FRC equilibria have been computed[5] with comparable magnitude of B_ϑ as that observed experimentally. These equilibria show a minor reduction in $\langle\beta\rangle$ but almost no change in the equilibrium structure (axial distribution of flux surfaces). However, it seems unlikely that the observed B_ϑ was an equilibrium quantity in view of its fluctuating character.

Conclusions. During the process of translation, FRCs appeared to maintain a relatively robust structure which efficiently moved particles, flux, and energy from one coil to another. These are encouraging results for the proposed FRX-D experiment as well as for eventual reactor applications.

X. Formation

Field-Reversed Theta Pinch. The sequence of stages that occur during formation of an FRC have been described elsewhere.[3] Useful analytic models and numerical methods have been developed to describe the process quantitatively.[22,58,61] Despite the research carried out in the area of formation and relatively good success in the laboratory at forming FRC configurations, the experimental approach still tends to be an empirical process of trial and error with strong dependences on the details of preionization in ways that have yet to be clarified.

The pulsed high-voltage power needed to extrapolate the theta pinch to a fusion reactor has generally been regarded as a drawback for the FRC concept. Alternatively, the rotating magnetic field method[62] of FRC formation and the slow coaxial theta pinch[63,64] have potential for development as methods that require lower voltages. These are issues that will be resolved by further research. Regardless of the reactor relevance of the field-reversed theta pinch, this formation method is a proven and effective means for producing FRCs in the laboratory for the purpose of experimental investigations.

Experimental limitations to trapped flux. An important aspect of the field-reversed theta pinch formation process is the trapping of poloidal flux. Increased flux increases the value of x_s in a given experiment, and the reduction of average beta associated with larger x_s is expected to improve particle confinement as a result of reduced density gradients.[30] Futhermore, the

limitation that results from flux loss itself is also of concern as discussed in Sec. VII. Experimental methods to maintain the poloidal flux after the FRC is formed in a theta pinch (neutral beams and rotating magnetic fields or other forms of rf current drive) have been considered but have not yet been implemented experimentally. Thus, the lifetime determined by flux loss in pulsed theta-pinch experiments at this time is primarily determined by the amount of flux that can be trapped in the formation process.

In FRX-C the formation process has received relatively little attention until recently when a series of experiments was initiated to investigate z-discharge preionization.[65] This work is not yet complete, but indications so far are that the limitation of trapping flux in FRX-C is not directly related to preionization details. The problem is rather related to the strength of axial contraction, which increases in intensity as the amount of trapped flux increases. Above a certain level in trapped flux the axial contraction becomes so strong that the FRC fails to remain intact during the peak of the axial contraction.

Green-Newton Flux. It is readily seen in the analysis of the dynamic formation process that a characteristic flux, often termed the Green-Newton flux,[66] is defined by the initial experimental parameters:

$$\Phi^*(\mathrm{kG\text{-}cm^2}) = 7.1\left[E_\vartheta(\mathrm{kV/cm})\right]^{1/2}\left[p_o(\mathrm{mtorr})\right]^{1/4}\left[r_t\right]^2 \qquad (4)$$

where E_ϑ is the electric field initially applied to the theta-pinch coil, p_o is the initial fill pressure, and r_t is the discharge tube radius. In Fig. 23 the poloidal flux trapped in various experiments is compared to this characteristic flux. It is readily seen that the trapped flux tends to increase with increases in the characteristic flux and indeed this tendency can be seen in all models of formation. The solid line depicts a linear dependence. The points labeled LSM (a proposed upgrade to FRX-C) and FRX-D are predicted using the Steinhauer model[61] assuming that the strength of axial contraction, as monitored by the minimum elongation, is held fixed. These data also show that the balloon or programmed-formation method[67,68] results in increased trapped flux in devices of

relatively small size and thus small characteristic flux. A critical issue to be resolved by future experiments and theoretical studies is how the trapped flux scales with increased size, and whether or not the scaling is dependent on the use of programmed formation, particular methods of preionization, or other details of the formation method.

XI. ture Plans – FRX-D

Critical Issues. Based on the results obtained on FRX-C as well as other FRC experiments around the world, a number of well defined issues have emerged for future investigations. The most critical of these are the following:

- Particle Confinement
- Stability
- Flux losses
- Electron thermal conduction

The goal of experimental work should be to address these issues in a regime of plasma parameters that resembles the reactor regime to as great an extent as possible. An important parameter that has recently been identified[68] is $\bar{s}$, the effective number of ion gyroradii between the field null and the separatrix.

The $\bar{s}$ Parameter. In the FRC, as in any magnetic confinement configuration, a useful characteristic is the number of ion gyroradii that exist between the peak of the plasma pressure profile and the outer boundary of the confined plasma. In most toroidal configurations the minor radius is an obvious dimension and the characteristic gyroradius is easily defined. In the FRC the characteristic dimensions and gyroradius are influenced by the high-beta nature of the equilibrium. Near the field null the gyroradius approaches infinity, and the effective number of gyroradii depends in detail upon the internal distribution of magnetic field between the field null and the separatrix. When these high-beta effects are taken into account,[68] one finds that an appropriate estimate of the effective number of gyroradii is given by the formula:

$$\bar{s} = \int_R^{r_s} \frac{r\, dr}{r_s \rho_i}, \qquad (5)$$

where ρ_i is evaluated at the local magnetic field within the FRC. In those cases where the ion temperature can be approximated as uniform in radius, the value of $\bar{s}$ can equally well be expressed:

$$\bar{s} = \frac{\varphi}{2\pi\, r_s\, \rho_{io}\, B_w}, \tag{6}$$

where φ is the poloidal flux. In other words, the integral that allows estimation of the number of gyroradii is just the flux integral. As mentioned earlier, the flux can be shown to be bounded by limits for the elongated type of equilibria that characterize present experiments. These limits give the following range of $\bar{s}$ values in terms of easily measured quantities:

$$\bar{s}_{min} = \frac{x_s^2}{4\sqrt{2}} \frac{R}{\rho_{io}} \qquad (\varepsilon = -1) \tag{7}$$

$$\bar{s}_{max} = \frac{x_s}{4} \frac{R}{\rho_{io}} \qquad (\varepsilon = 0) \tag{8}$$

To obtain a better estimate within these limits, one must determine the internal distribution of B(r) by measurements or by theoretical models such as one-dimensional transport calculations. Notice that the high-beta magnetic structure in an FRC has the consequence of reducing the effective number of ion orbits by one order of magnitude compared with the ratio of characteristic size to gyroradius (R/ρ_{io}).

Although the parameter $\bar{s}$ is rather difficult to determine experimentally, it is emerging as an extremely important characteristic which can be used to distinguish between qualitatively different regimes of FRC phenomena. Present experiments have values of $\bar{s}$ which are less than two,[5] whereas transport models predict that adequate confinement to meet the Lawson condition will require $\bar{s}$ of about 30.[30,69] The improvement in particle confinement as $\bar{s}$ increases[70] is seen explicitly in an analytical transport model[69] based on LHD resistivity. In

Fig. 24 the prediction of particle confinement time τ_N based on Ref. 69 is plotted vs. $\bar{s}$ for parameters that would be representative of the next generation of experiments. It is apparent that with $\bar{s}$ in the range of 6 to 7, the particle confinement time would approach one millisecond.

Internal Tilting. The prediction of a fast-growing internal tilt mode (n = 1 ballooning mode) seems to be unavoidable with n the context of the MHD model.[71] The conjecture for many years that the stabilization might be due to strong kinetic effects associated with the ion motion in the high beta FRC has been substantiated by recent theoretical results.[72] In calculations that use the Vlasov model for ions and cold, massless electrons, it is found that the dominant stabilizing effect comes from the superthermal portion of the Maxwellian distribution. At small $\bar{s}$ these high energy particles have orbits large enough to sample the open magnetic field lines whose average curvature is good for stability. As $\bar{s}$ increases the effect diminishes. Thus the growth rate from the kinetic calculation normalized to the MHD growth rate (Fig. 25) increases with $\bar{s}$. The growth rate in the present regime of $\bar{s}$ ($\bar{s} < 2$) is suppressed by more than an order of magnitude from the MHD value. It would appear from this theory that the mode has not been seen experimentally because the mode is only weakly unstable for small $\bar{s}$. In any case the assumptions that go into the stability analysis are no longer valid when the growth time of the instability becomes comparable to transport time sceles. Collisions and plasma rotation are neglected, the electron temperature is zero, and the eigenfunction for the unstable mode needs to be determined more accurately. Only one equilbrium has been examined, and it differs is some respects with the equilibrium determined experimentally. Finally, the stability theory is only linear, and the nonlinear consequences of the instability will have to be determined either from experiment or 3-D particle simulation (no suitable code exists at this time).

FRX-D Facility. A new experiment has been proposed recently by Los Alamos[73] to address the critical issues of confinement and stability in the new regime of increased $\bar{s}$. To investigate flux loss and thermal conduction at increased temperatures, the FRX-D facility also includes significant plasma heating by adiabatic compression. The proposed experiment, shown in Fig. 26, accomplishes the formation, heating, and final trapping of the FRC in three independent coils. Formation is done in a large diameter (1.3 m) high-voltage coil with four feed plates arranged similarly to FRX-C. The purpose of the high

voltage is to ensure trapping adequate flux. The energy of the high-voltage capacitor bank (about 1 MJ) and the magnetic field in the formation region (about 4 kG) are kept small, because after formation the plasma is translated into the compression coil where the FRC is then heated by adiabatic compression using a lower-voltage capacitor bank (ignitron-switched 10-kV capacitors). The process of translation improves the efficiency of adiabatic compression, because the bias field and dimensions of the compression coil are chosen so that the FRC nearly fills the entire coil before compression. After compression the FRC is translated a second time into the third coil, which consists of a dc solenoid with a metal vacuum chamber. The dc fields in the third chamber, which is actually the existing FRX-C/T translation vessel, eliminate the need for an expensive and complicated power crowbar system in the compression coil. Such a system would be required for the plasma lifetimes expected in the compressor. The second translation into the third coil also permits adjustment of the final value of the x_s, which allows some increase of the value of $\bar{s}$. Parameters projected for the FRX-D device are listed in Table VII.

Conclusion. The results of research on FRX-C along with the substantial progress on FRCs from elsewhere around the world have clearly defined the issues that need to be addressed in a new generation of experiments. The research to date has been carried out in relatively small devices that are far from the regime of relevance to a fusion reactor. Although the uncertainties are numerous, as one would expect given the limited resources that have so far been devoted to FRC research, the prospects for a qualitatively different and improved type of fusion reactor give strong motivation for constructing new facilities capable of addressing the various critical issues.

REFERENCES

1. R. L. HAGENSON and R. A. KRAKOWSKI, "A Compact-Toroid Fusion Reactor (CTOR) Based on the Field-Reversed Theta Pinch," Fusion Reactor Design and Technology, Vol. 1, IAEA, Vienna (1983) 377.

2. C. C. BAKER, et al., "Starfire – A Commercial Tokamak Fusion Power Plant Study," ANL/FPP-80-1, Argonne National Laboratory (September, 1980).

3. W. T. ARMSTRONG, R K. LINFORD, D. A. PLATTS, and E. G. SHERWOOD, "Field-Reversed Experiments (FRX) on Compact Toroids," Phys. Fluids 24 (1981) 2068.

4. V. N. SEMENOV and N. V. SOSNIN, "Characteristic Equilibrium States of a Compact Plasma Toroid," Sov. J. Plasma Phys. 7 (1981) 180.

5. R. L. SPENCER and M. TUSZEWSKI, "Experimental and Computational Equilibria of FRCs," Phys. Fluids (accepted for publication, 1985).

6. M. TUSZEWSKI, W. T. ARMSTRONG, R. R. BARTSCH, R. E. CHRIEN, and J. C. COCHRANE, et al. "Flux Loss During the Equilibrium Phase of Field-Reversed Configurations," Phys. Fluids 25 (1982) 1696.

7. R. L. SPENCER, M. TUSZEWSKI and R. K. LINFORD, "Adiabatic Compression of Elongated Field-Reversed Configurations," Phys. Fluids 26 (1983) 1564.

8. A. C ES KOV, R. KH. KURTMULLAEV, A. P. KRESHCHUK, YA. N. LAUKHM, and A. I. MALYUTIN, et al., "Principles of Plasma Heating and Confinement in a Compact Toroidal Configuration," Proceedings of the Sixth European Conference on Controlled Fusion and Plasma Physics, Moscow, USSR, Vol. I (1973) 599.

9. A. EBERHAGEN and W. GROSSMAN, "Theta Pinch Experiments With Trapped Anti Parallel Magnetic Field," Z. Physik 248 (1971) 130.

10. J. L. SCHWARZMEIER, D. C. BARNES, D. W. HEWETT, C. E. SEYLER, AND A. I. SHESTAKOV, et al., "Magnetohydrodynamic Equlibrium and Stability of Field-Reversed Configurations," Phys. Fluids 26 (1983) 1295.

11. D. S. HARNED and D. W. HEWETT, "The Origin of Rotation in Field-Reversed Configuration," Nucl. Fusion 24 (1984) 201.

12. W. T. ARMSTRONG, D. C. BARNES, R. R. BARTSCH, R. J. COMMISSO, AND C. A. EKDAHL, et al., "Compact Toroid Experiments and Theory," in Plasma Physics and Controlled Nuclear Fusion Research (Proc. 8th Int. Conf. Brussels, 1980) Vol. 1, IAEA, Vienna (1981) 481.

13. L. C. STEINHAUER, "Plasma Rotation in Reversed-Field Theta Pinches," Phys. Fluids 24 (1981) 328.

14. Y. ASO, Ch. WU, S. HIMENO, and K. HIRANO, "End Effects on the n = 2 Rotational Instability in the Reversed-Field Theta-Pinch," Nucl. Fusion 22 (1982) 843.

15. H. DREICER, "Proposal for FRX-C and Multiple Cell Compact Torus Experiments," LA-8045-P, Los Alamos National Laboratory (October 1979).

16. T. MINATO, M. TANJYO, S. OKADA, Y. ITO, and M. KAKO, et al., "Experimental Studies on Confinement of Field-Reversed-Configuration Plasma," in Plasma Physics and Controlled Nuclear Fusion Research (Proc. 9th Int. Conf. Baltimore, 1982) Vol. 2, IAEA, Vienna (1983) 303.

17. S. OHI, T. MINATO, Y. KAWAKAMI, M. TANJYO, and S. OKADA, et al., "Quadrupole Stabilization of the n = 2 Rotational Instability of a Field-Reversed Theta Pinch Plasma," Phys. Rev. Lett. 51 (1983) 1042.

18. A. L. HOFFMAN, J. T. SLOUGH, and D. G. HARDING, "Suppression of the n=2 Rotational Instability in Field-Reversed Configurations," Phys. Fluids 26 (1983) 1626.

19. R. E. CHRIEN, W. T. ARMSTRONG, R. R. BARTSCH, J. C COCHRANE, AND R. W. KEWISH, et al., "Quadrupole Stabilization of the n=2 Rotational Mode in FRX-C," Conference Record of the IEEE International Conference on Plasma Science, San Diego (1983) paper 6P8.

20. R. W. KEWISH, JR., R. R. BARTSCH, and R. E. SIEMON, "Engineering Design of the FRX-C Experiment," 9th Symposium for Engineering Problems of Fusion Research, Chicago, Illinois (October 26-29, 1981).

21. R. E. SIEMON, W. T. ARMSTRONG, R. R. BARTSCH, R. E. CHRIEN, and J. C. COCHRANE, et al., "Experimental Studies of Field-Reversed-Configuration (FRC) Confinement in FRX-C," in Plasma Physics and Controlled Nuclear Fusion Research (Proc. 9th Int. Conf. Baltimore, 1982) Vol. 2, IAEA, Vienna (1983) [illegible].

22. R. E. SIEMON and R. R. BARTSCH, "Scaling Laws for FRC Formation and Prediction of FRX-C Parameters," Third Symposium on the Physics and Technology of Compact Toroids (Los Alamos, NM 1980), LA-8700-C, 172.

23. D. J. REJ, "Design and Construction Details of the FRX-C/T Device: A Compact Toroid Plasma Translation Experiment," LA-10108-MS, Los Alamos National Laboratory (August 1984).

24. M. TUSZEWSKI, "Experimental Study of the Equilibrium of Field-Reversed Configurations," Plasma Phys. Contr. Fusion 26 (1984) 991.

25. D. J. REJ and W. T. ARMSTRONG, "Electron Temperature Measurements in the Field-Reversed Configuration Experiment FRX-C," Nucl. Fusion 24 (1984) 177.

26. K. F. McKENNA, W. T. ARMSTRONG, R. R. BARTSCH, R. E. CHRIEN, AND J. C. COCHRANE, et al., "Particle Confinement Scaling in Field-Reversed Configurations," Phys. Rev. Lett. 50 (1983) 1787.

27. M. TUSZEWSKI, "Excluded Flux Analysis of a Field-Reversed Plasma," Phys. Fluids 24 (1981) 2126.

28. D. W. HEWETT and R. L. SPENCER, "Two-Dimensional Equilibria of Field-Reversed Configurations in a Perfectly Conducting Cylindrical Shell," Phys. Fluids 26 (1983) 1299.

29. D. E. SHUMAKER, "Numerical Calculation of Compact Torus Equilibria," J. Comput. Phys. 53 (1984) 456.

30. M. TUSZEWSKI and R. K. LINFORD, "Particle Transport in Field-Reversed Configurations," Phys. Fluids 25 (1982) 765.

31. D. J. REJ, "Interaction of the Neutral Deuterium Flux with a Field-Reversed Configuration," Proceedings of the Sixth U. S. Symposium on Compact Toroid Research (Princeton, New Jersey 1984) 214.

32. M. TUSZEWSKI and W. T. ARMSTRONG, ""Simplified Diamagnetic Techniques for a Field-Reversed Theta-Pinch Plasma," Rev. Sci. Instrum. 54 (1983) 1611.

33. M. TUSZEWSKI and K. F. McKENNA, "Interpretation of End-On Interferometry in Field-Reversed Configurations," Phys. Fluids 27 (1984) 1058.

34. S. HAMASAKI and N. A. KRALL, "Anomalous Diffusion Calculations in Field-Reversed Configurations," Conference Record of the IEEE International Conference on Plasma Science (IEEE Publishing Service, Montreal, 1979) 143.

35. R. E. SIEMON, W. T. ARMSTRONG, R. E. CHRIEN, P. L. KLINGNER, AND R. K. LINFORD, et al., "Theoretical Studies of Field-Reversed Configurations (FRCs) and Experimental Study of the FRC During Translation," in Plasma Physics and Controlled Nuclear Fusion Research (Proc. 10th Int. Conf. London, 1984) IAEA, Vienna (1985, to be published) paper DIII-2-1.

36 L. C. STEINHAUER, R. D. MILROY, and J. T. SLOUGH, "A Model For Inferring Transport Rates From Observed Confinement Times In Field-Reversed Configurations," submitted to Phys. Fluids (1984).

37. T. ISHIMURA, "Multipole-Field Stabilization of the Rotational Instability in a Theta Pinch," Phys. Fluids 27 (1984) 2139.

38. Y. NOGI, S. SHIMAMURA, and S. HAMADA, "Stabilization of FRC Plasma by Helical Quadrupole Field," Japan-US Joint Symposium on Compact Toroid Research, Hiroshima, Japan (November 13-15, 1984).

39. M. TANJYO, S. OKADA, Y. ITO, M KAKO, and S. OHI, et al., "Stabilization and Translation of a Plasma with Field Reversed Configuration," in Plasma Physics and Controlled Nuclear Fusion Research (Proc. 10th Int. Conf. London, 1984) IAEA, Vienna (1985, to be published) paper DIII-2.

40. H. P. FURTH and C. LUDESCHER, "Stellarator Hybrids," Fizika Plazmy, (to be published, 1985).

41. D. S. HARNED, "Suppression of the n=2 Rotational Instability in the Field-Reversed Configuration By Means of Quadrupole Fields," Phys. Fluids 27 (1984) 544.

42. R. L. SPENCER and M. TUSZEWSKI, "MHD Equilibrium and Stability of Rotating FRCs With Excluded Multipole Field," Phys. Fluids 28 (1985) accepted for publication.

43. D. J. REJ and M. TUSZEWSKI, "A Zero-Dimensional Transport Model for Field-Reversed Configurations," Phys. Fluids 27 (1984) 1514.

44. Y. ASO, S. HIMENO, and K. HIRANO, "Experimental Studies on Energy Transport in a Reversed Field Theta Pinch," Nucl. Fusion 23 (1983) 751.

45. E. H. KLEVANS, "Zero-Dimensional Modeling of Field-Reversed Theta-Pinch Machines," Proceedings of the US-Japan Joint Symposium on Compact Toruses and Energetic Particle Injection (Princeton, 1979) 126.

46. D. E. SHUMAKER, J. K. BOYD, S. P. AUERBACH, and B. M. McNAMARA, "Numerical Simulations of Transport in a Field-Reversed Mirror Mirror Plasma," J. Comput. Phys. 45 (1982) 266.

47. S. HAMADA, "A Model of Equilibrium Transport and Evolution of Field-Reversed Configuration," Submitted to Nuclear Fusion (1985).

48. M. Y. HSIAO, E. J. CARAMANA, and J. L. SCHWARZMEIER, "A One-Dimensional Transport Code for Field-Reversed Configurations," Bull. Am. Phys. Soc. 29 (1984) 1327.

49. M. TUSZEWSKI,"1-D Transport Model for FRCs," Proc. 1983 Sherwood Mtg. (Arlington, VA) paper 1Q4.

50. K. F. McKENNA and R. E. CHRIEN, "Radiative Energy Loss Measurements on Translating Field-Reversed Configurations (FRCs)," Bull. Am. Phys. Soc. (1984) 1328.

51. R. E. CHRIEN, K. F. McKENNA, D. J. REJ, and M. TUSZEWSKI, "Radiation and Impurity Measurements in FRX-C/T," Japan-US Joint Symposium on Compact Toroid Research, Hiroshima, Japan (November 13-15, 1984).

52. A. L. HOFFMAN, R. D. MILROY, and L. C. STEINHAUER, "Poloidal Flux Loss in a Field-Reversed Theta Pinch," Appl. Phys. Lett. 41 (1982) 31.

53. M. TUSZEWSKI, W. T. ARMSTRONG, R. E. CHRIEN, P. L. KLINGNER, and K. F. McKENNA, et al., "Confinement of Translating Field-Reversed Configurations (FRCs)," Bull. Am. Phys. Soc. (1984) 1328.

54. D. J. REJ, M. TUSZEWSKI, W. T. ARMSTRONG, R. E. CHRIEN, and P. L. KLINGNER, et al., "FRC Translation Dynamics and Plasma Confinement Properties in FRX-C/T," Japan-US Joint Symposium on Compact Toroid Research, Hiroshima, Japan (November 13-15, 1984).

55. S. G. ALIKHANOV, V. P. BAKHTIN, A. G. ES'KOV, R. KH. KURTMULLAEV, and V. N. SEMENOV, et. at., "Three-Dimensional Plasma Compression in a Z-Pinch Liner System-Transport and Compression of a Compact Torus by a Quasi-Spherical Liner," in Plasma Physics and Controlled Nuclear Fusion Research (Proc. 9th Int. Conf. Baltimore, 1982) Vol. 3, IAEA, Vienna (1983) 319.

56. D. J. REJ, M. R. PARKER, and H. H. FLEISCHMANN, "Measurements of Resistive Wall and Plasma Drag on the Axial Translation of Field-Reversing E-Layers," Phys. Fluids 26 (1983) 323.

57. M. TANJYO, S. OKADA, Y ITO, M KAKO, and S. OHI, et al., "Translation Experiment of a Plasma with Field Reversed Configuration," Technology Reports of the Osaka University, 34 (1984) 201.

58. R. D. MILROY and J. U. BRACKBILL, "Numerical Studies of a Field-Reversed Theta-Pinch Plasma," Phys. Fluids 25 (1982) 775.

59. W. T. ARMSTRONG, R. E. CHRIEN, K. F. McKENNA, D. J. REJ, and E. G. SHERWOOD, et al., "Internal Magnetic Field Measurements in a Translating Field-Reversed Configuration," Proceedings of the 6th U. S. Symposium on Compact Toroid Research 1984 (Princeton, NJ) 218.

60. W. T. ARMSTRONG and R. E. CHRIEN, "Internal Field Probing of Translating FRCs," Japan-US Joint Symposium on Compact Toroid Research, Hiroshima, Japan (November 13-15, 1984).

61. L. C. STEINHAUER, "Plasma Heating in Field-Reversed Theta Pinches," Phys. Fluids 26 (1983) 254.

62. E. DURANCE, B. L. JESSUP, I. R. JONES, and J. TENDYS, "Experimental Observations of Rotomak Equilibria," Phys. Rev. Lett. 48 (1982) 1253.

63. K. F. McKENNA and R. F. GRIBBLE, "The Coaxial Slow Source: A Quasi-Static FRC Formation Concept," Proceedings of the 6th U. S. Symposium on Compact Toroid Research 1984 (Princeton, NJ) 202.

64. K. D. HAHN and G. C. VLASES, "Modeling of a Coaxial FRC Slow Source," ibid, 198.

65. W. T. ARMSTRONG, K. F. McKENNA, R. E. CHRIEN, D. J. REJ, and E. G. SHERWOOD, et al., "Formation of FRCs With Large x_s in FRX-C/T," Bull. Am. Phys. Soc. 29 (1984) 1328.

66. T. S. GREEN and A. A. NEWTON, "Diffusion of Antiparallel Bias Magnetic Field during the Initial Stages of a Theta-Pinch," Phys. Fluids 9 (1966) 1386.

67. V. V. BELIKOV, V. M. GOLOVIZNIN, V. K. KORSHUNUV, A. P. KRESHUK, and R. K. KURTMULLAYEV, et al., "Suppression of Losses in a Compact Torus With Programmed Shaping of the Magnetic Structure," in Plasma Physics and Controlled Nuclear Fusion Research (Proc. 9th Int. Conf. Baltimore, 1982) Vol. 2, IAEA, Vienna (1983) 343.

68. J. T. SLOUGH, A. L. HOFFMAN, R. D. MILROY, D. G. HARDING, and L. C. STEINHAUER, "Flux and Particle Life-Time Measurements in Field-Reversed Configurations," Nucl. Fusion 24 (1984) 1537.

69. A. L. HOFFMAN, R. D. MILROY, "Particle Lifetime Scaling in Field-Reversed Configurations Based on Lower-Hybrid Drift Resistivity," Phys. Fluids 26 (1983) 3170.

70. R. K. LINFORD, "Los Alamos Compact Toroid, Fast Liner, and High Density Z-Pinch Programs," in Unconventional Approaches to Fusion, B. Brunelli and G. G. Leotta, Eds., (Plenum Press, New York, 1982) 463.

71. J. L. SCHWARZMEIER, and C. E. SEYLER, "Inadequacies of Finite Larmor Radius Treatments of the Internal Tilting Instability in Field-Reversed Configurations," Phys. Fluids 27 (1984) 2161.

72. J. L. SCHWARZMEIER, H. R. LEWIS, D. C. BARNES, and C. E. SEYLER, "Unstable Modes of Multidimensional Vlasov Equilibria: Stability of Field-Reversed Configurations," Bull. Am. Phys. Soc. 29 (1984) 1327.

73. The Los Alamos FRC Group, "Proposal for the FRX-D Large $\bar{s}$ Adiabatic-Compression Experiment," LA-UR 84-3371, Los Alamos National Laboratory (November, 1985).

TABLE I: Representative FRX-B Parameters
17 mtorr

Machine:		
Coil radius	r_w	12.5 cm
Magnetic field	B_w	6.5 kG
Electric field	E_ϑ	0.41 kV/cm
Coil length	L	1.0 m
Fill pressure	p_o	17 mtorr
Bias field	B_l	2.2 kG
Plasma:		
Separatrix radius	r_s	5 cm
x_s	x_s	0.4 → 0.5
Ion [illegible]ature	T_i	200 eV
Electron temperature	T_e	110 eV
Density	n	3.5×10^{15} cm^{-3}
Stable period	τ_{obs}	30 μs
Particle loss time	τ_N	39 μs

TABLE II: FRX-C Device Parameters

Coil geometry	
Central coil Radius (1.6 m long)	0.25 m
Mirror Region Radius (0.2 m each end)	0.22 m
Magnetic mirror ratio	1.17
Coil length	2.0 m
Discharge tube ID	0.40 m
Magnetic Field	
Main Field (vacuum, no bias)	10.5 kG
Rise time ($\tau/4$)	4.5 μs
Decay time (L/R in vacuum)	300 μs
Electric field, E_θ	0.41 kV/cm
Bias field (adjustable)	0 → 4 kG
Energy storage	
Main bank (140 2.8-μf caps)	397 kJ 45 kV
Bias bank (10.2 mF)	326 kJ 8 kV

TABLE III: Representative FRX-C Plasma Parameters

		5 mtorr	20 mtorr
Magnetic field(kG)	B_w	8	7
Bias field(kG)	B_l	0.7	1.6
Separatrix radius(cm)	r_s	9	10
x_s	x_s	0.36	0.40
Separatrix length(cm)	ℓ_s	130	150
Ion temperature(eV)	T_i	625	150
Electron temperature(eV)	T_e	175	100
Density(10^{15} cm^{-3})	n	1.9×10^{15}	5×10^{15}
Stable period(μs)	τ_{obs}	30 → 70	55 → 110
Particle loss time(μs)	τ_N	67±25	154±25
Energy loss time(μs)	τ_E	35	80
Flux loss time(μs)	τ_φ	250	180

TABLE IV: Quantities used in O-D Model

	Definition	Method of Measurement
B_w	External field	Magnetic probes
T	$T_e + T_i$	Pressure balance
T_e	Electron temperatures	Thomson scattering
T_i	Ion temperature	Pressure balance
V	Volume	Magnetic probes
n	$\int n d\ell / 2r_s$	Side on interferometer; r_s from magnetic probes
r_s	Separatrix radius	Magnetic probes
N	Electrons contained in separatrix	Two methods - see text

TABLE V. Flux Confinement Scaling $\tau_\varphi \sim \ell^a x_s^b n_M^c T^d$

	a	b	c	d	
Classical	0	2	0	1.5	(T_e)
FRX-C/T	-1±0.6	2.0±0.6	0.2±0.4	0.2±0.3	$(T_i + T_e)$
TRX-1*	-	2.0	0.3	-0.1	$(T_i + T_e)$

*each exponent is the average of those of good and bad PI data.

TABLE VI: Adiabatic compression laws

Plasma quantity	Adiabatic scaling*
ℓ_s	$x_s^{2(3-\varepsilon-\gamma)/\gamma}\ (1-\frac{x_s^2}{2})^{-(1+\varepsilon-\gamma\varepsilon)/\gamma}\ r_w^{2/5}$
T_M	$x_s^{-2(3-\varepsilon)(\gamma-1)/\gamma}\ (1-\frac{x_s^2}{2})^{(1+\varepsilon)(\gamma-1)/\gamma}\ r_w^{-8/5}$
n_M	$x_s^{-2(3-\varepsilon)/\gamma}\ (1-\frac{x_s^2}{2})^{-(1+\varepsilon)(\gamma-1)/\gamma}\ r_w^{-12/5}$
B_w	$x_s^{-3+\varepsilon}\ r_w^{-2}$

*In these laws $\gamma = 5/3$

TABLE VII: FRX-D Parameters

	Formation	Compression	Confinement
r_w(cm)	64	37	17.5
x_s	0.55	0.6→0.52	0.8
ℓ_s(m)	2.6	5.7→1.9	4.2
$n_M(10^{15}\ cm^{-3})$	1.0	0.8→4.7	5.0
$T_e = T_i$ (eV)	188	150→521	500
B (kG)	4.0	3.2→14.1	14.1
$\bar{s}$ (LHD)	4.2	5.6→4.6	6.5
E_p (kJ)	80	64→221	212
Coil Voltage (kV)	200	10	dc
Fill (mtorr)	5.5		
Bias Field (kG)	1		

FIGURES

Fig. 1 Field reversed configuration geometry in a theta pinch coil, showing the closed field lines of the FRC within the separatrix radius r_s, the open field line region outside the separatrix, the quartz vacuum vessel, and the coil with its passive mirrors.

Fig. 2 Comparison of the external B field measured in FRX-A and FRX-B between the quartz tube and the coil at the axial midplane. Traces are shown for both vacuum and a static 5 mtorr D_2 fill pressure.

Fig. 3 Schematic of the FRX-C field reversed theta pinch.

Fig. 4 Photograph of the FRX-C/T confinement region showing dc coils and a portion of the theta pinch coil.

Fig. 5 Radial $\int ndl$ profile at z=0 for 20 mtorr. The solid circles are experimental data. The curves correspond to (a) parabolic, (b) uniform, and (c) modeled FRC density profiles.

Fig. 6 Axial profiles of $\int ndl$ and $r_{\Delta\varphi}$ at 20 mtorr. in the middle of the equilibrium phase. The open and solid circles are experimental data for $r_{\Delta\varphi}/r_{\Delta\varphi}(0)$ and $\int ndl/\int ndl(0)$, respectively. The dashed curves are elliptical and racetrack contours.

Fig. 7 End-on interferogram of an FRC formed with 20 mtorr fill pressure shown within the quartz vacuum vessel and theta pinch coil.

Fig. 8 Scaling of particle confinement time τ_N with R^2/ρ_{i0}; open circles from end-on holography, triangles from side-on interferometry and $r_{\Delta\varphi}$ axial profile; and solid circles from Tuszewski-Linford lower hybrid transport model. The solid line is an empirical fit to the data.

Fig. 9 Time evolution of the total electron inventory measured with the holographic interferometer for (a) 20 mtorr and (b) 5 mtorr. The lines indicate the best fit to the exponential decay.

Fig. 10 End-on holographic interferograms of the FRC at two times showing the stabilizing effect of the quadrupole fields.

Fig. 11 Time evolution of the magnetic field, separatrix radius and length, average density, and pressure-balance temperature, with and without quadrupole fields, for the 20 mtorr fill pressure case.

Fig. 12 Time evolution of the magnetic field, separatrix radius and length, average density, and pressure-balance temperature, with and without quadrupole fields, for the 5 mtorr fill pressure case.

Fig. 13 Time evolution of the line-integrated density and rotational parameter α with and without quadrupole fields. The arrows indicate the time at which the quadrupole fields were applied.

Fig. 14 Time evolution of the magnetic field, separatrix radius and volume, average density, pressure-balance temperature, electron temperature from Thomson scattering, neutron emission, and electron inventory from side-on and end-on interferometry for the 5 mtorr fill pressure case, together with the zero dimensional modeling (dashed lines) of the data.

Fig. 15 Time evolution of the magnetic field, separatrix volume and radius, pressure-balance and Thomson scattering temperatures, average density, and electron inventory for the 20 mtorr fill pressure case, together with zero dimensional modeling (dashed lines) of the data.

Fig. 16 Radial profile of electron temperature measured by Thomson scattering, together with the prediction of a one dimensional energy transport model.

Fig. 17 Variation of x_s, separatrix length, and pressure-balance and electron temperatures with magnetic field, together with the predictions of adiabatic theory for the high (dashed line) and low (solid line) flux profiles.

Fig. 18 Schematic of the FRX-C/T translation experiment.

Fig. 19 Axial profile of the FRC separatrix radius at various times.

Fig. 20 Ratio of final - to - initial maximum density (a) and pressure-balance temperature (b) as a function of magnetic field ratio. The dashed lines are the predictions from adiabatic theory.

Fig. 21 Variation of the axial velocity of the translating plasma with the dc guide field in the translation vessels.

Fig. 22 Calculated poloidal flux surfaces from a 2-D MHD code used to model the FRX-C/T translation experiment. The time in microseconds is shown at the upper right corner of each frame.

Fig. 23 Variation of trapped flux with Green-Newton flux for various FRC experiments together with predictions for future experiments.

Fig. 24 Variation of particle confinement time with $\bar{s}$, predicted from the Hoffman-Milroy model based on lower hybrid drift transport.

Fig. 25 Variation of the growth rate for the internal tilt mode predicted by kinetic theory, normalized by the MHD rate, with $\bar{s}$. The dashed line is the approximate threshold for the mode to be observable during the FRC lifetime in FRX-C.

Fig. 26 Coil system for the proposed FRX-D experiment.

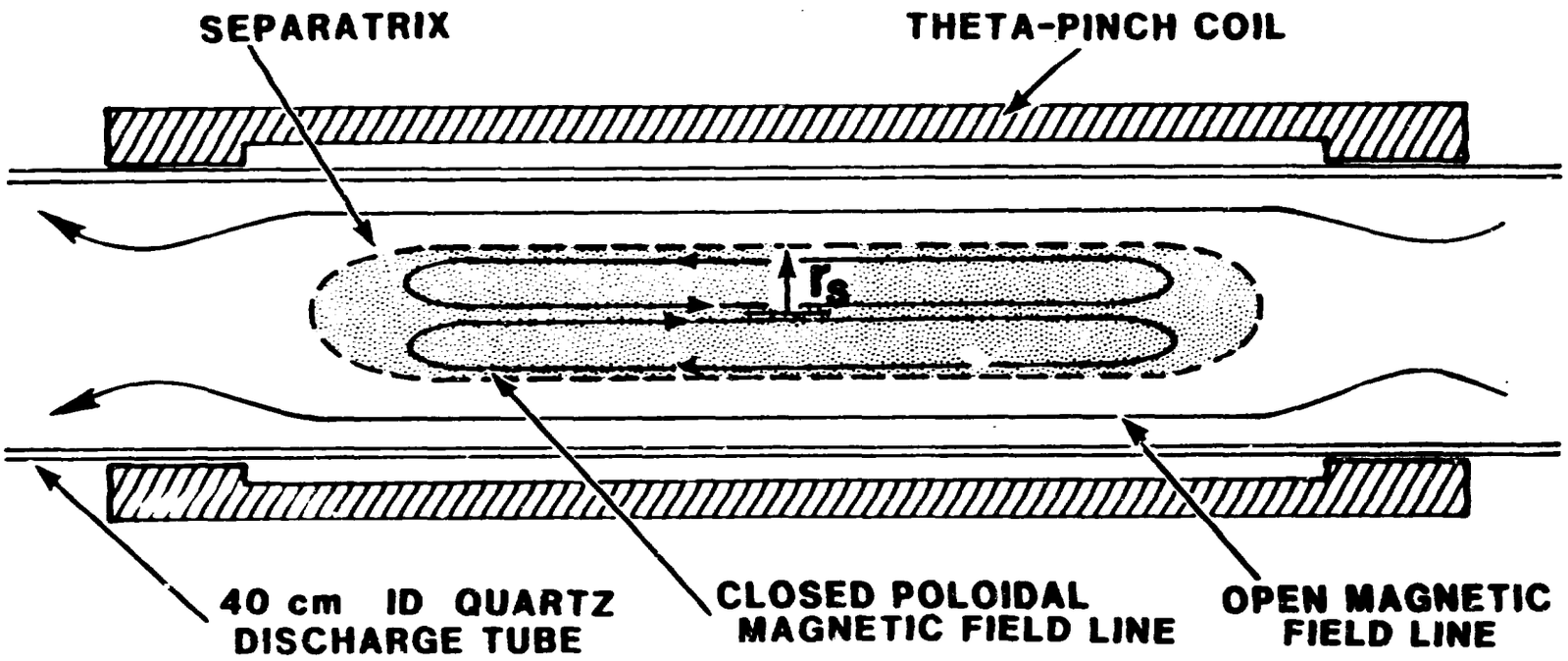
SEPARATRIX
THETA-PINCH COIL
r_s
40 cm ID QUARTZ
DISCHARGE TUBE
CLOSED POLOIDAL
MAGNETIC FIELD LINE
OPEN MAGNETIC
FIELD LINE

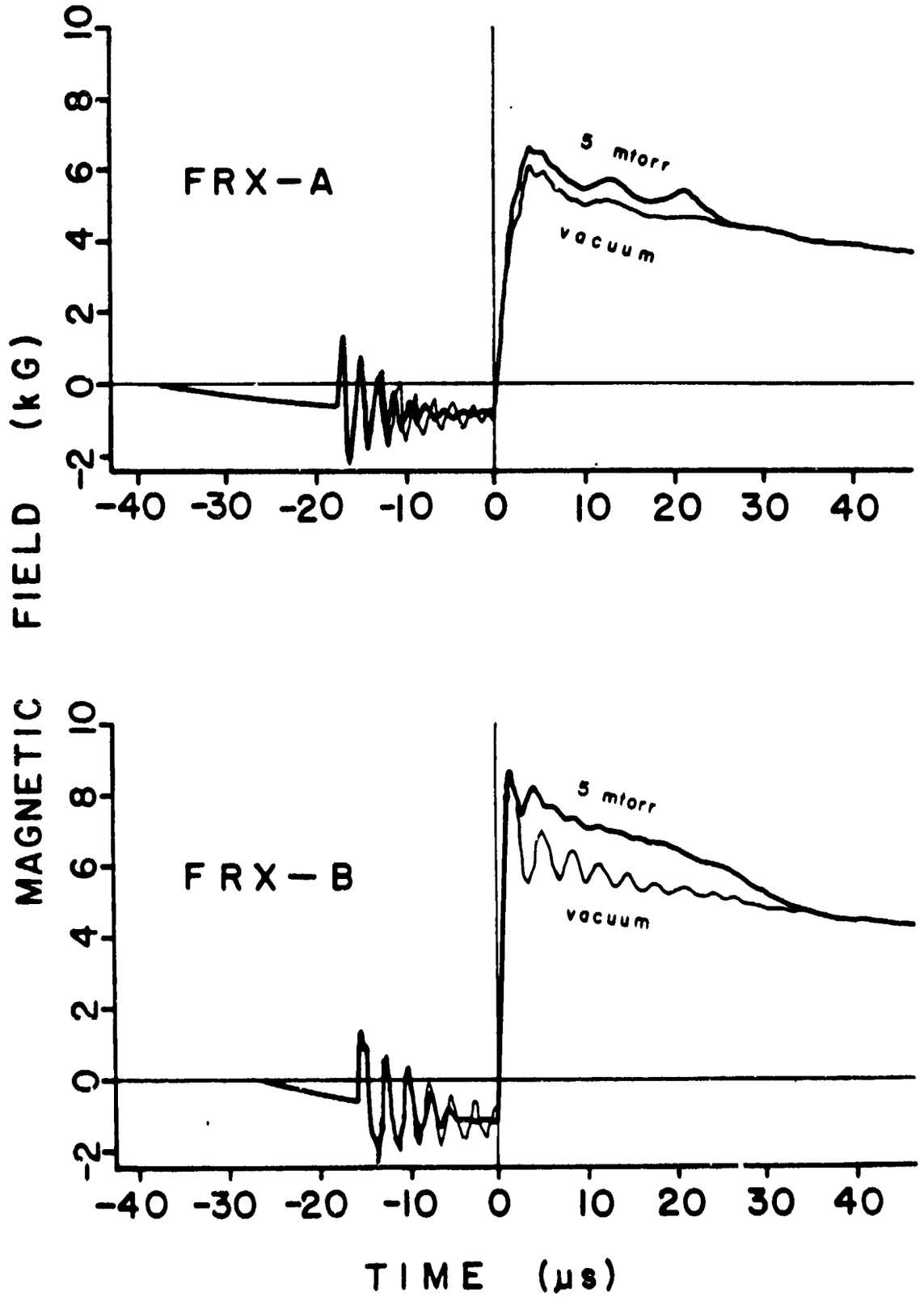
FRX-A
5 mtorr
vacuum
MAGNETIC FIELD (kG)
10
8
6
4
2
0
-2
-40 -30 -20 -10 0 10 20 30 40
FRX-B
5 mtorr
vacuum
TIME (μs)

Fig 2

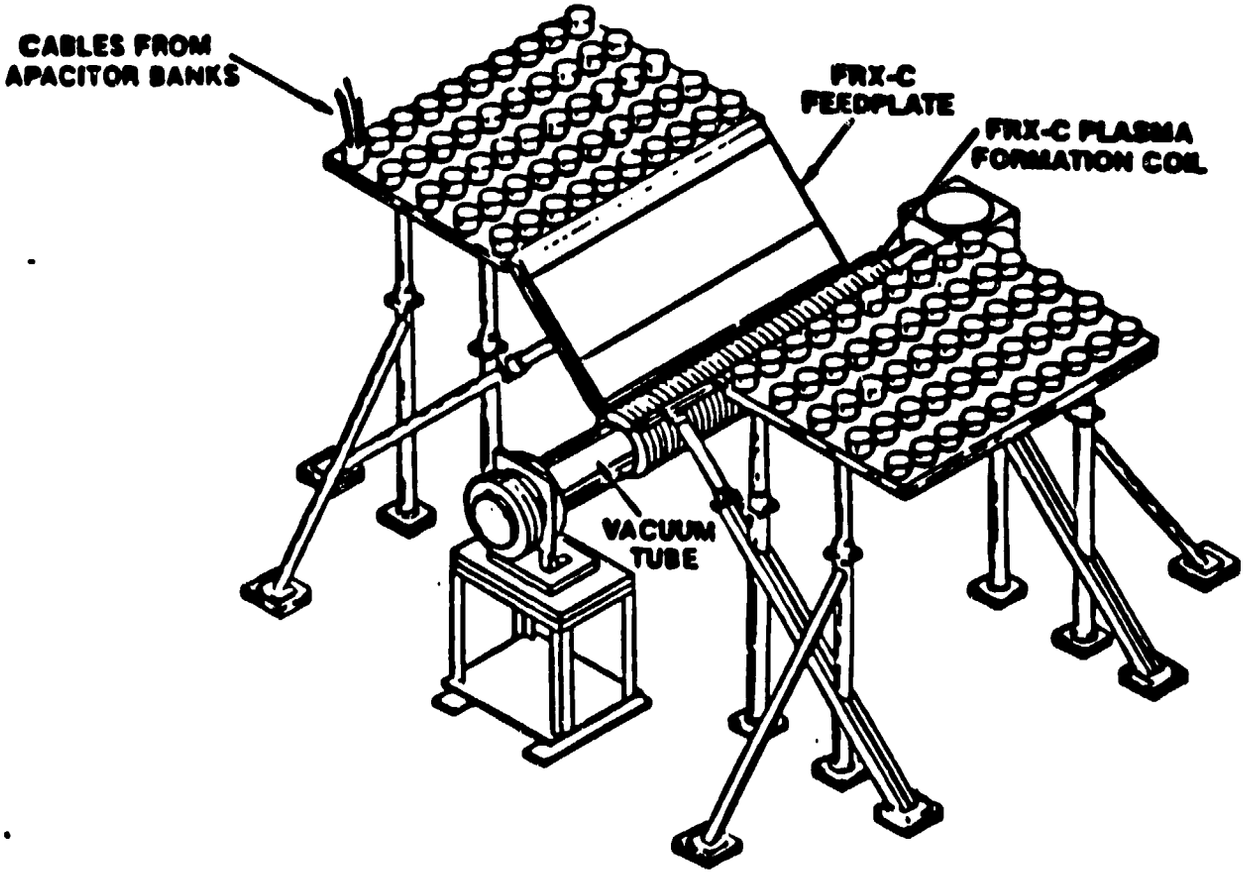
CABLES FROM
APACITOR BANKS
FRX-C
FEEDPLATE
FRX-C PLASMA
FORMATION COIL
VACUUM
TUBE

Fig 3

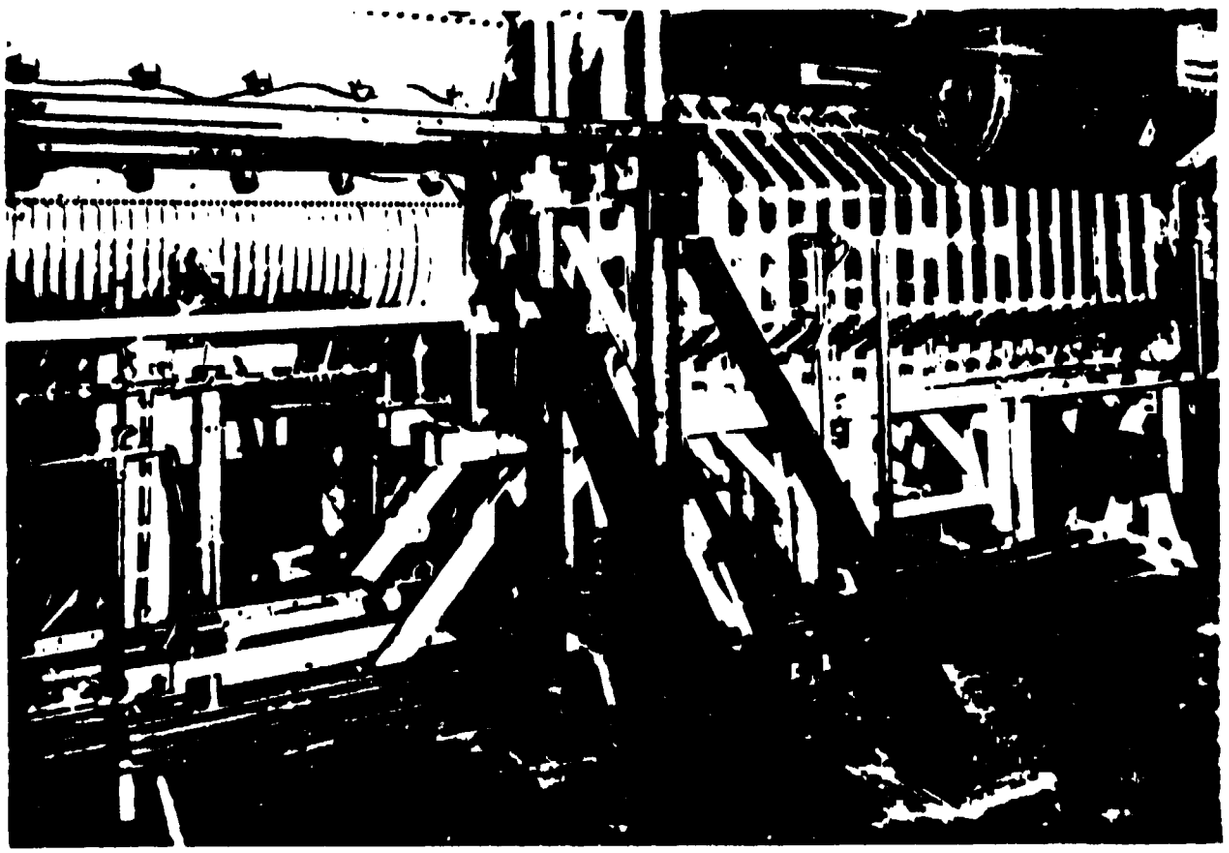

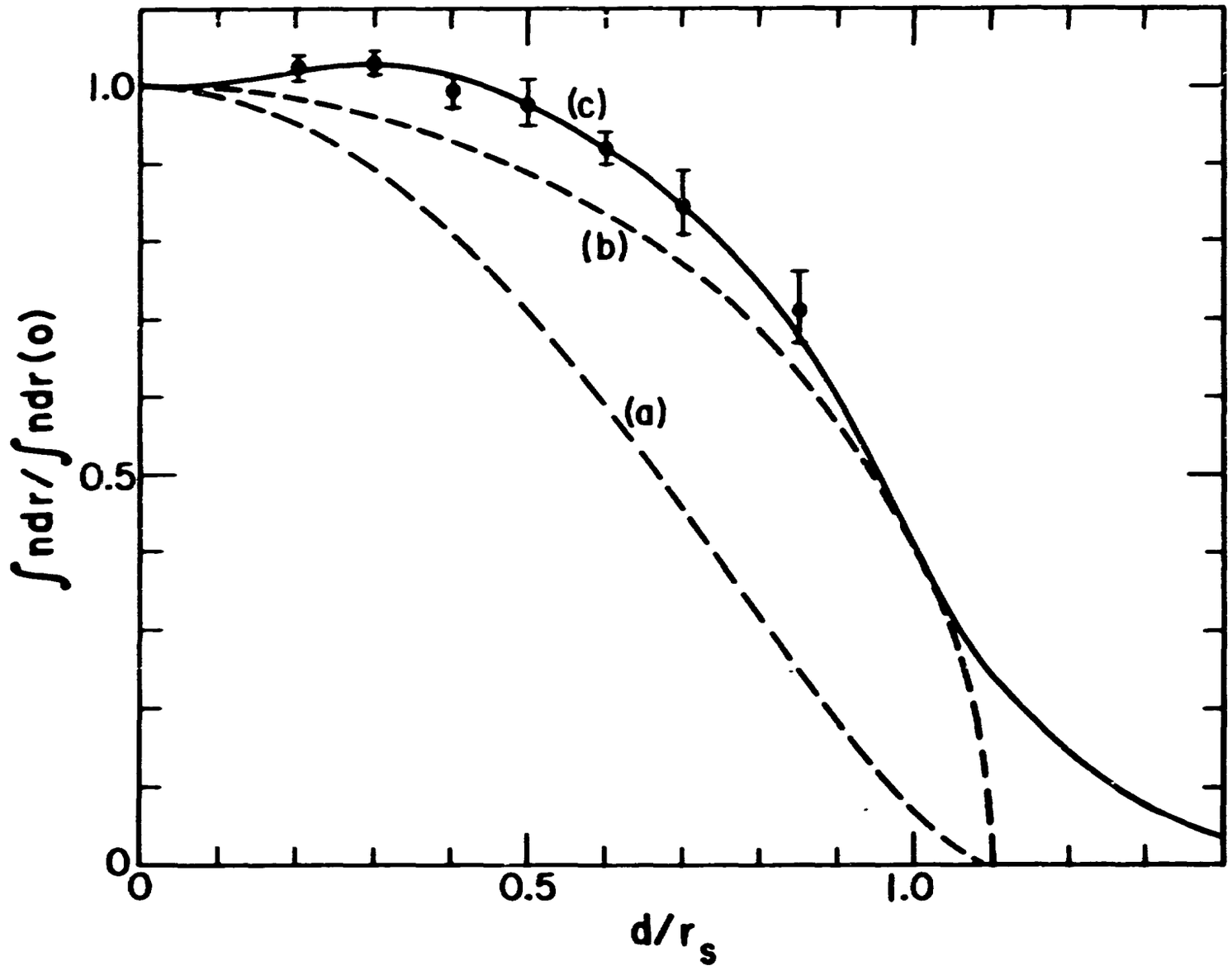
1.0
0.5
0
0
0.5
1.0
$\int ndr / \int ndr(o)$
d/r_s
(a)
(b)
(c)

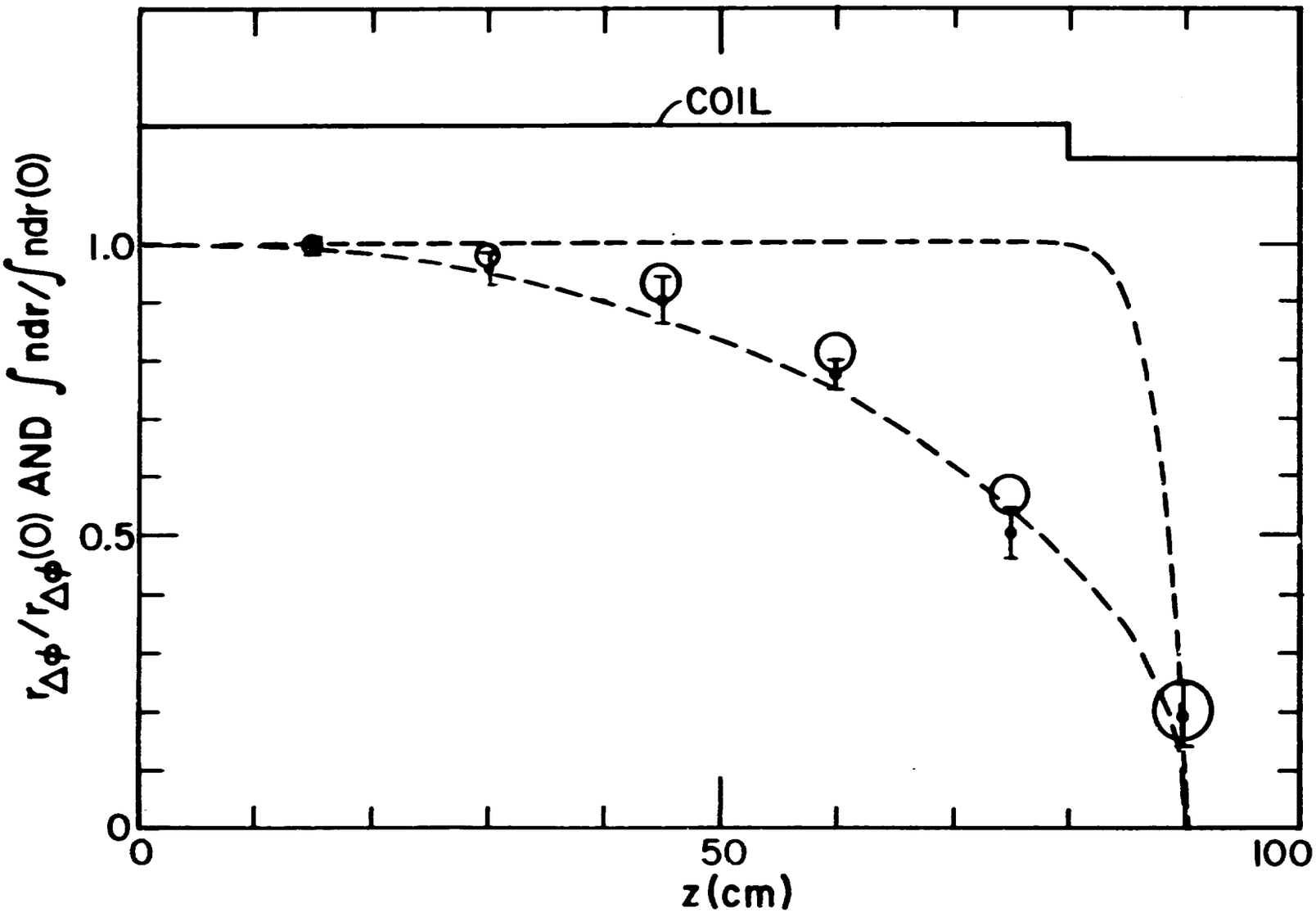
COIL
1.0
0.5
0
0
50
100
z(cm)
$r_{\Delta\phi}/r_{\Delta\phi}(0)$ AND $\int ndr/\int ndr(0)$

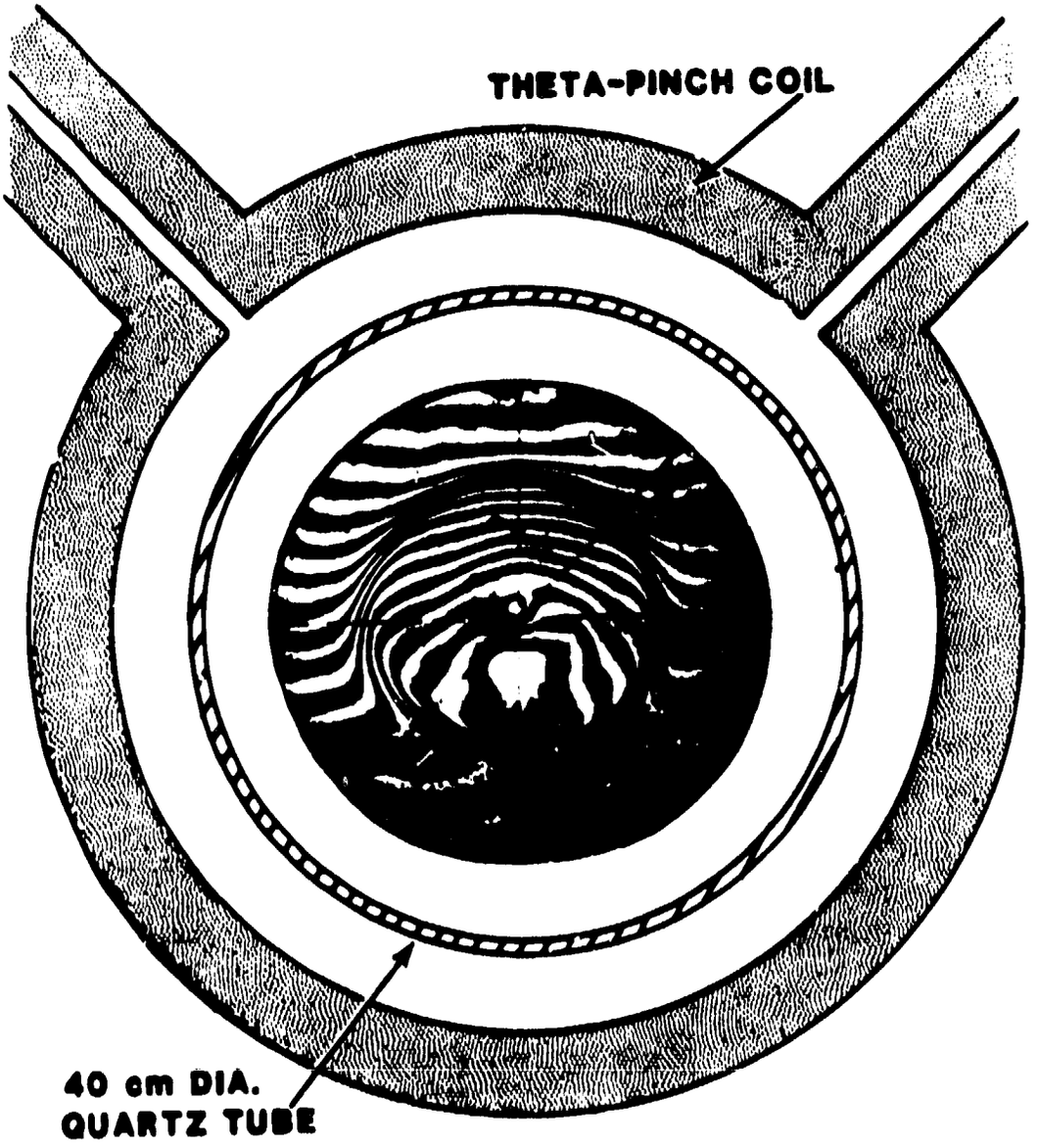

8/62C

Fig. 7

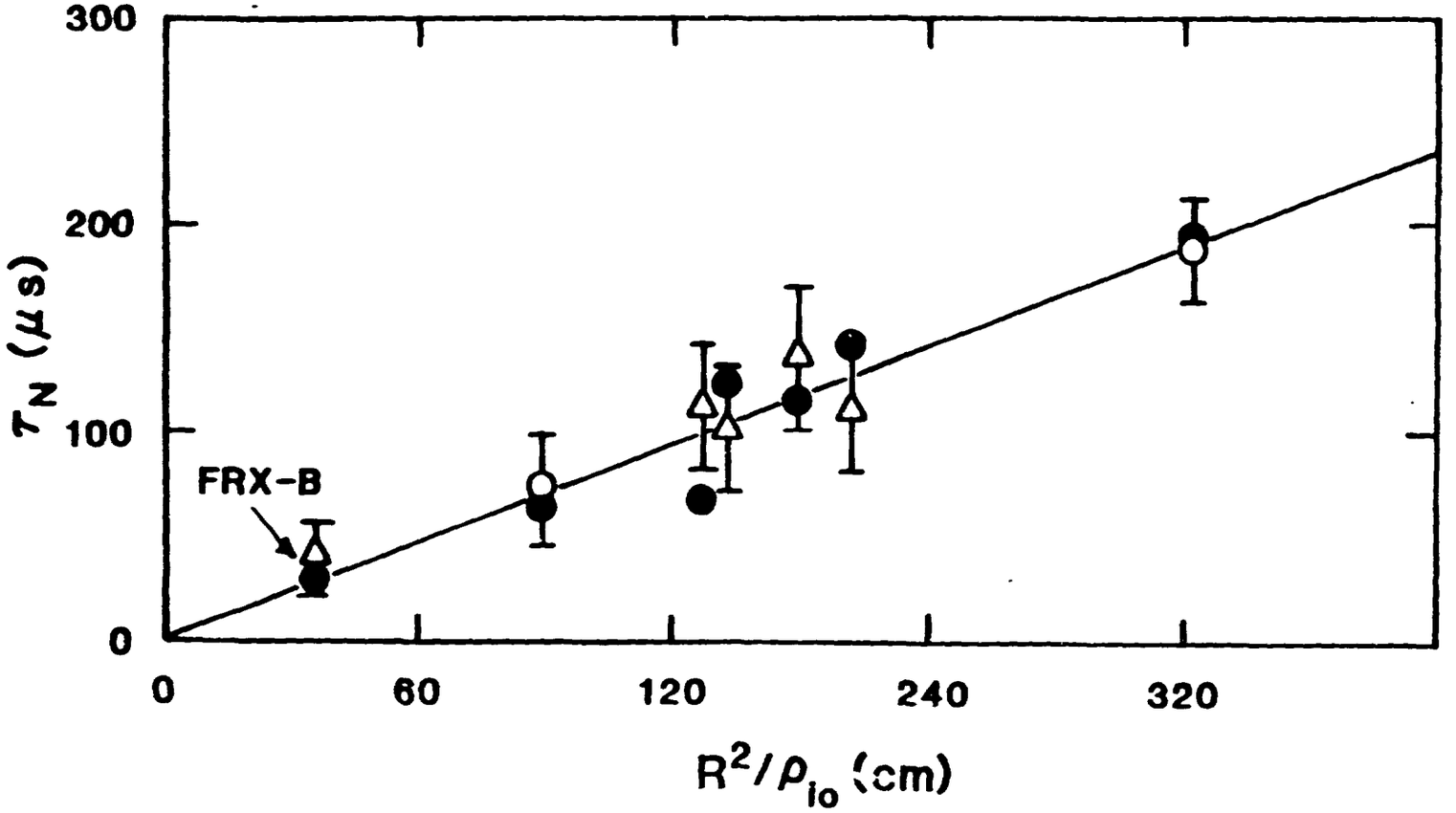
300
200
100
0
τ_N (μs)
FRX-B
0
60
120
240
320
R^2/ρ_{io} (cm)

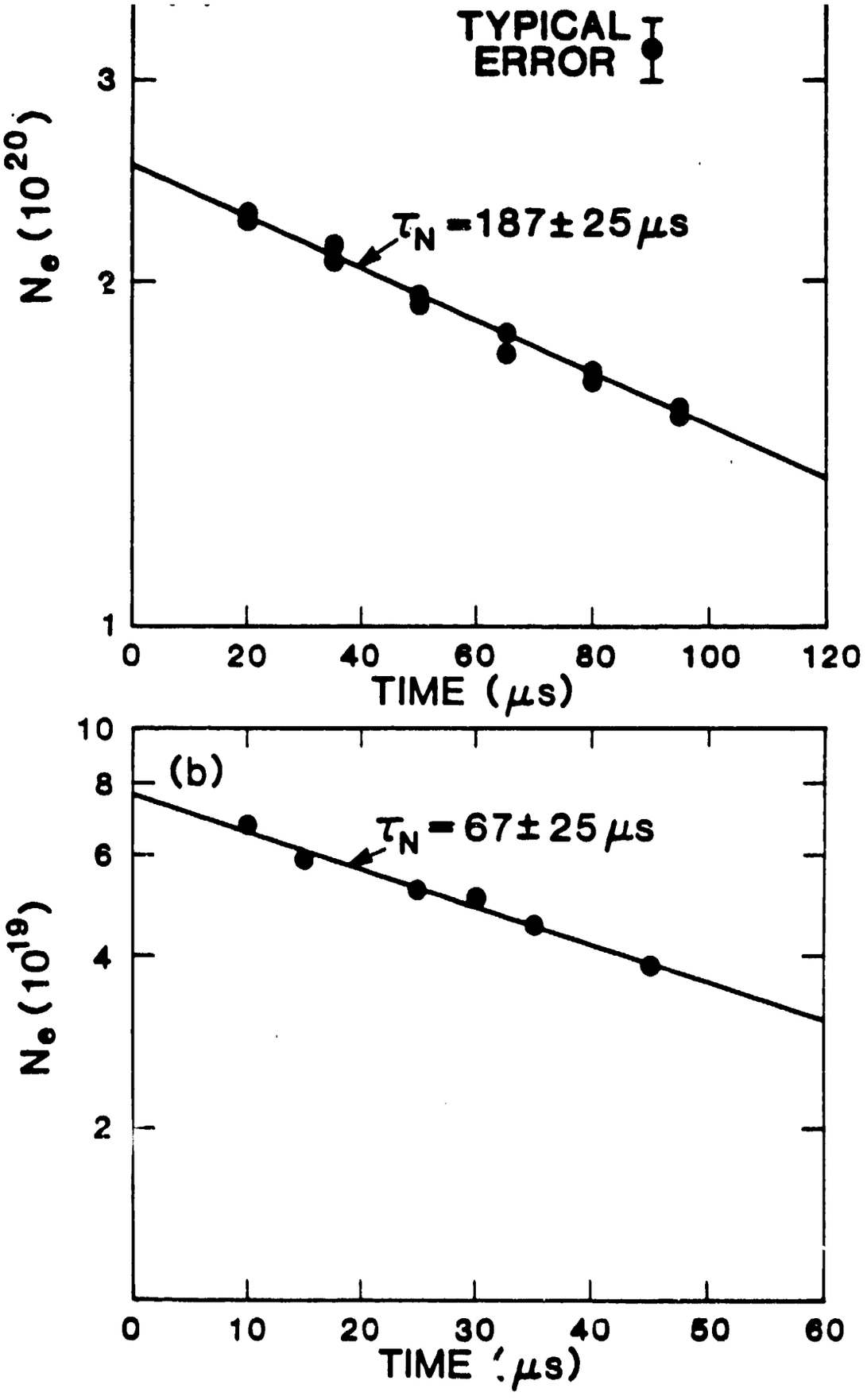

Fig. 9

3/85ctr5747

WITHOUT QUADRUPOLE FIELDS

WITH QUADRUPOLE FIELDS

t = 30 μs

t = 35 μs

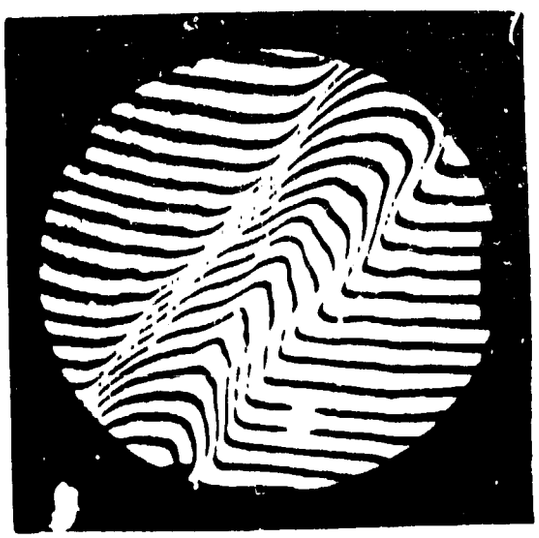

t = 110 μs

t = 110 μs

Fig. 10

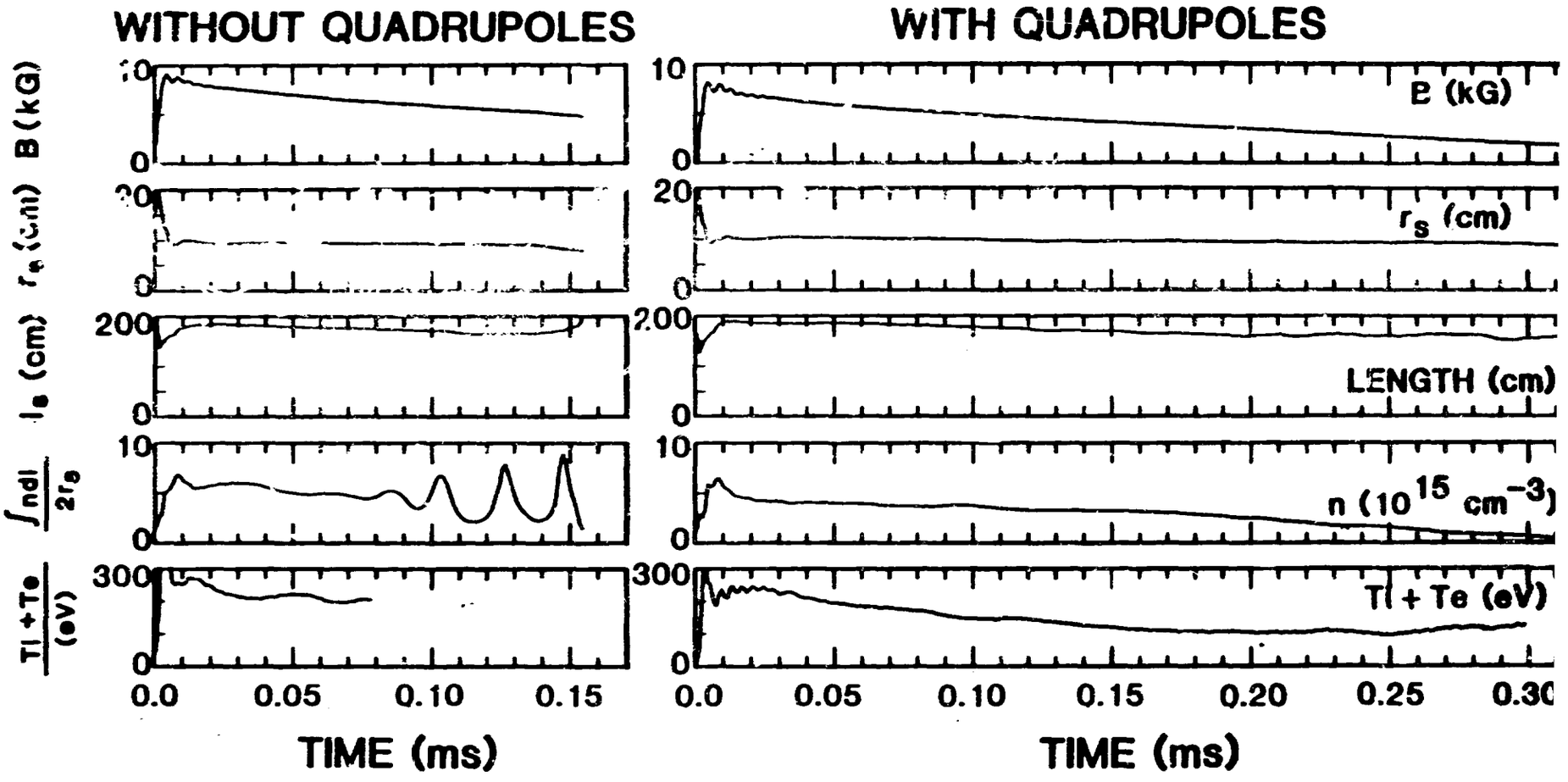
WITHOUT QUADRUPOLES
WITH QUADRUPOLES
B (kG)
r_s (cm)
l_e (cm)
$\frac{\int ndl}{2r_s}$
$\frac{Ti+Te}{(eV)}$
B (kG)
r_s (cm)
LENGTH (cm)
n (10^{15} cm^{-3})
Ti + Te (eV)
10
0
20
0
200
0
10
0
300
0
0.0
0.05
0.10
0.15
0.20
0.25
0.30
TIME (ms)
TIME (ms)

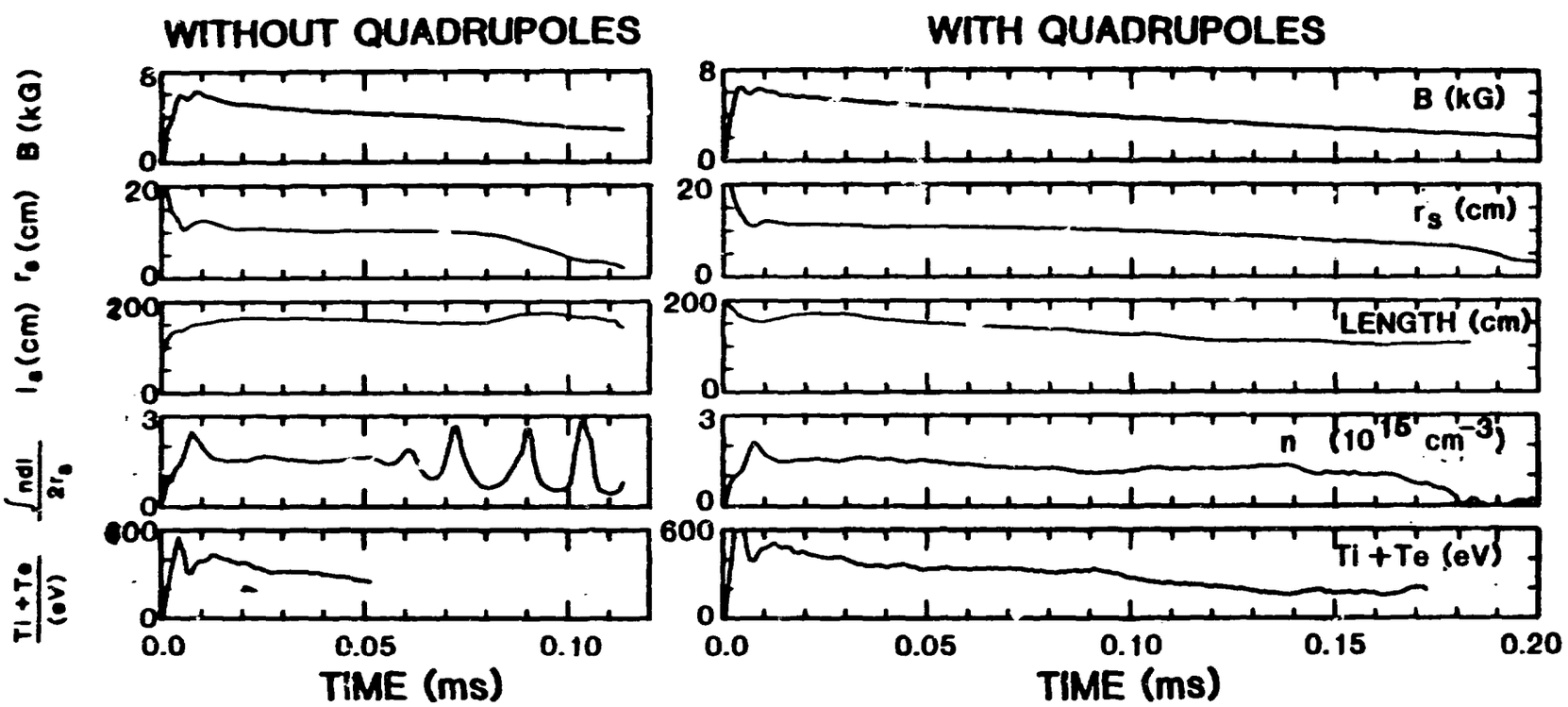
WITHOUT QUADRUPOLES
WITH QUADRUPOLES
B (kG)
r_s (cm)
LENGTH (cm)
n (10^{15} cm^{-3})
Ti + Te (eV)
l_e(cm) r_e(cm) B (kG)
$\frac{\int ndl}{2r_e}$
$\frac{Ti+Te}{(eV)}$
TIME (ms)
TIME (ms)

Fig. 12

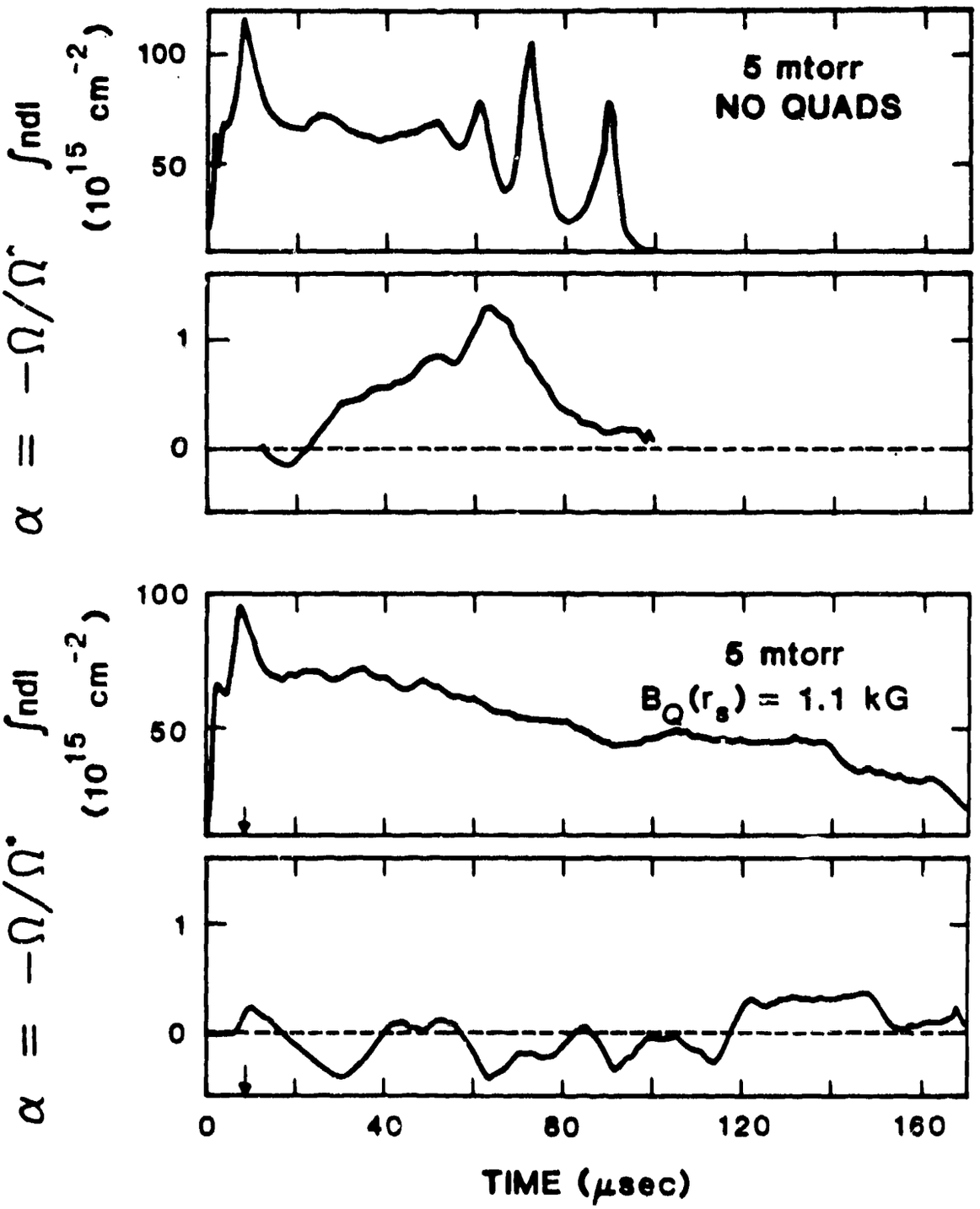

Fig. 13

3/83CTR3529

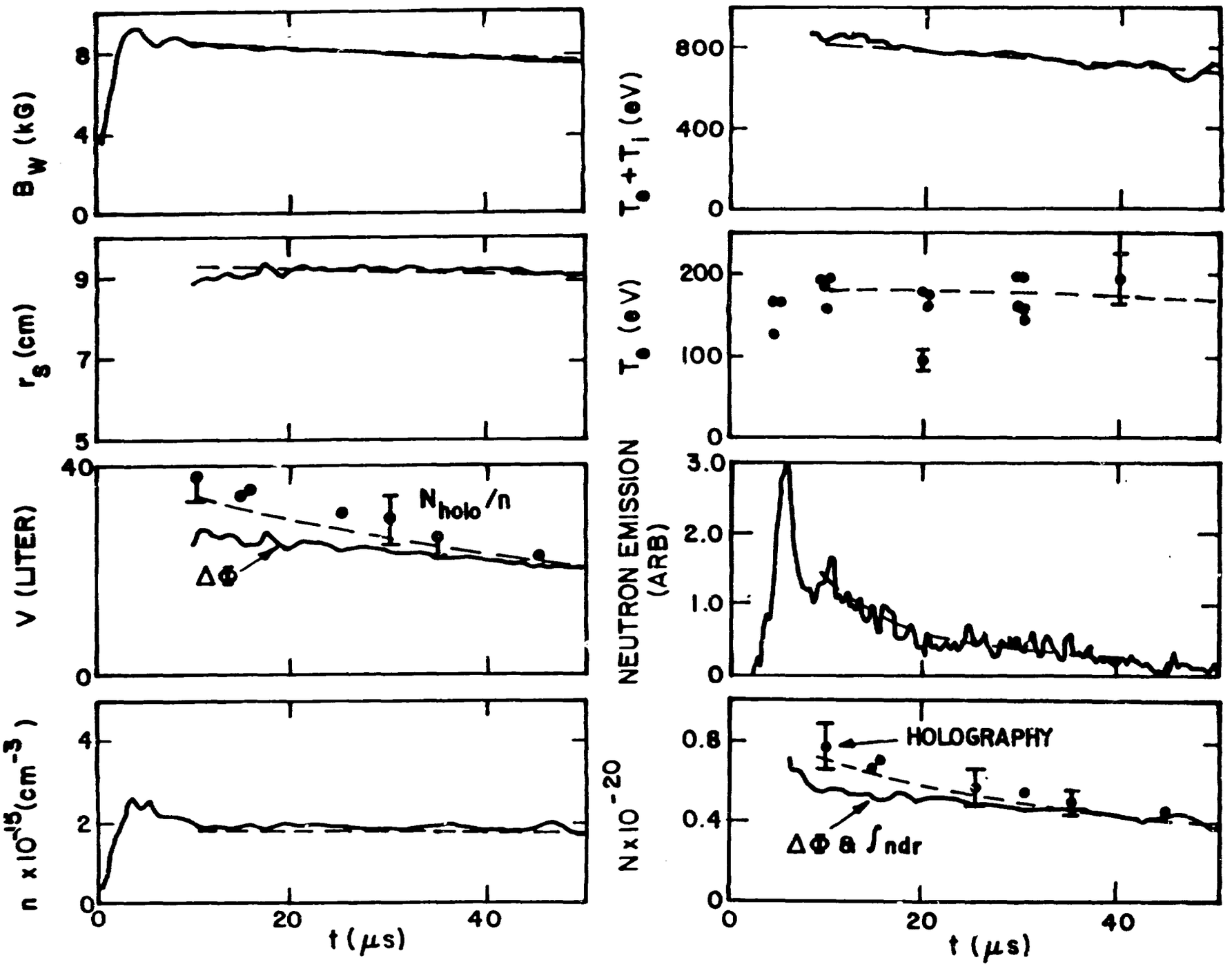
B_W (kG)
8
4
0
r_s (cm)
9
7
5
V (LITER)
40
0
N_{holo}/n
$\Delta\Phi$
n x 10^{-15} (cm^{-3})
4
2
0
0
20
40
t (μs)
T_e+T_i (eV)
800
400
0
T_e (eV)
200
100
0
NEUTRON EMISSION (ARB)
3.0
2.0
1.0
0
N x 10^{-20}
0.8
0.4
0
HOLOGRAPHY
$\Delta\Phi \propto \int ndr$
0
20
40
t (μs)

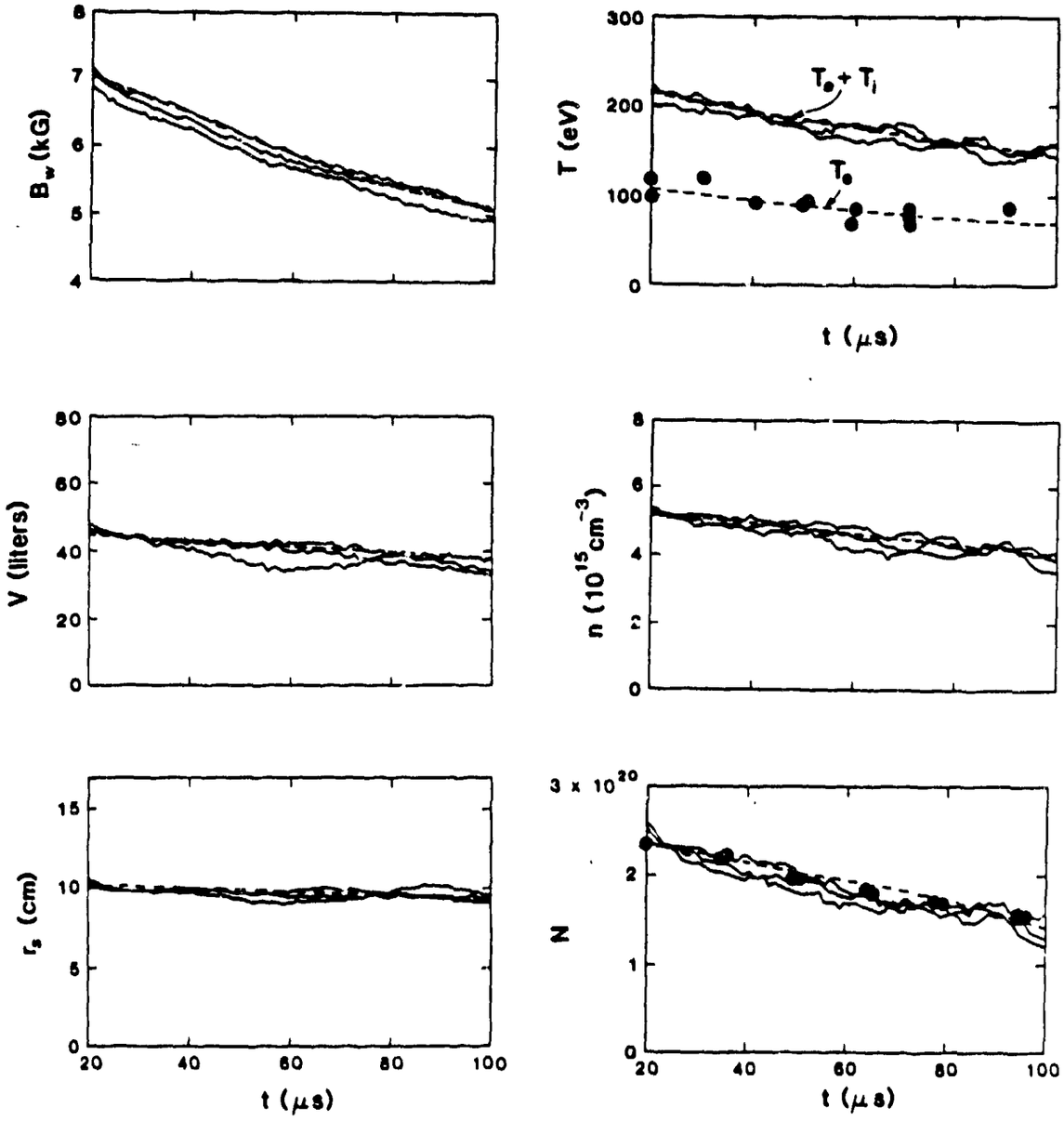

Fig. 15

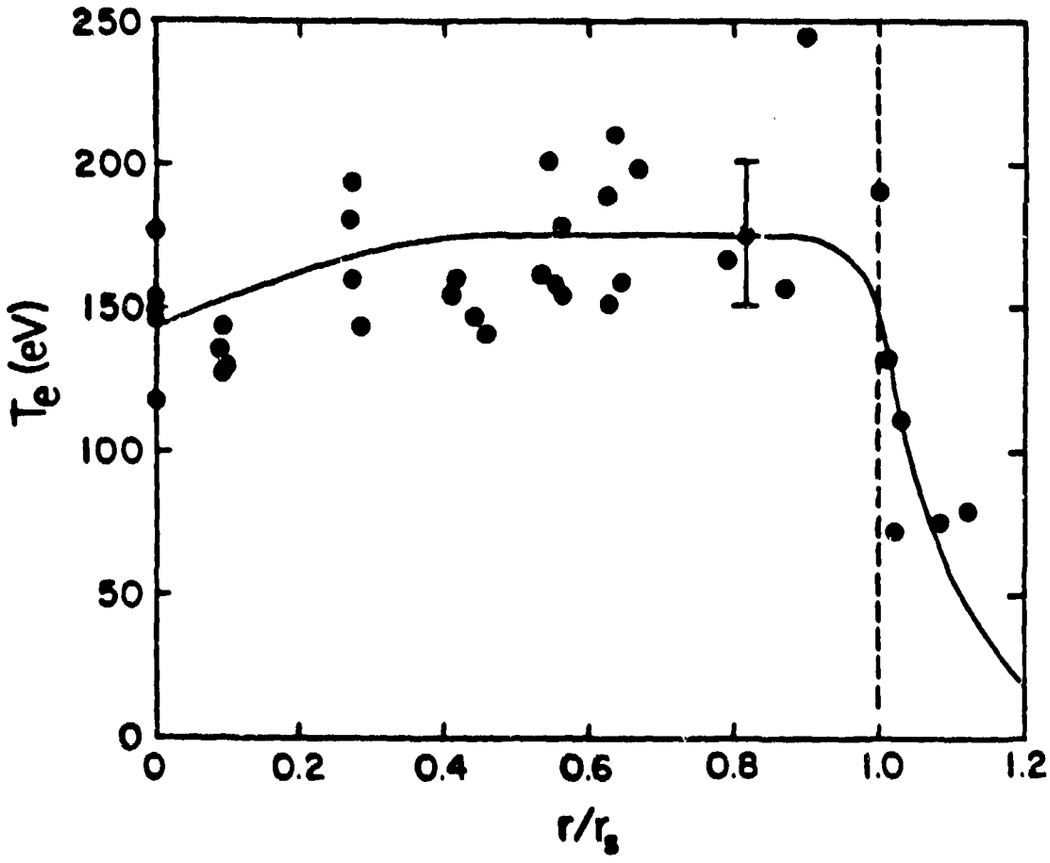

Fig. 16

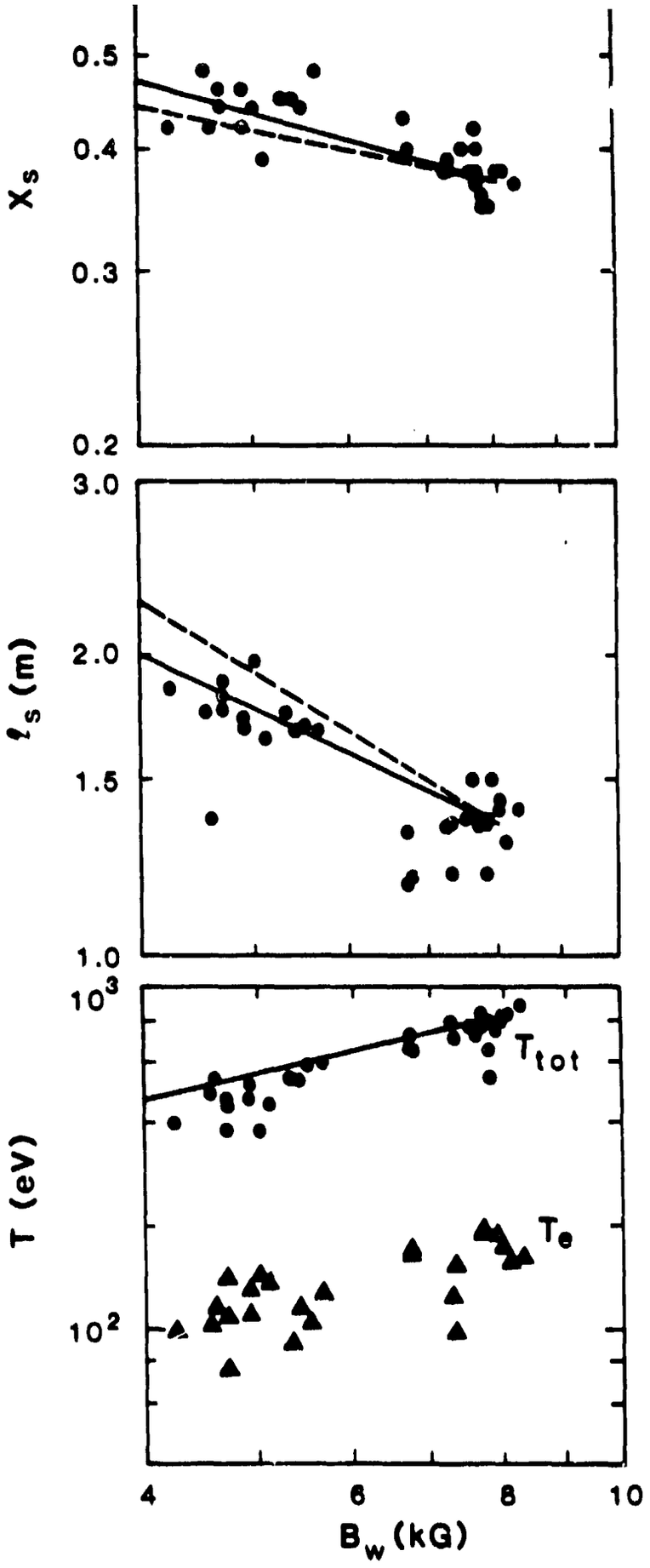

Fig. 17

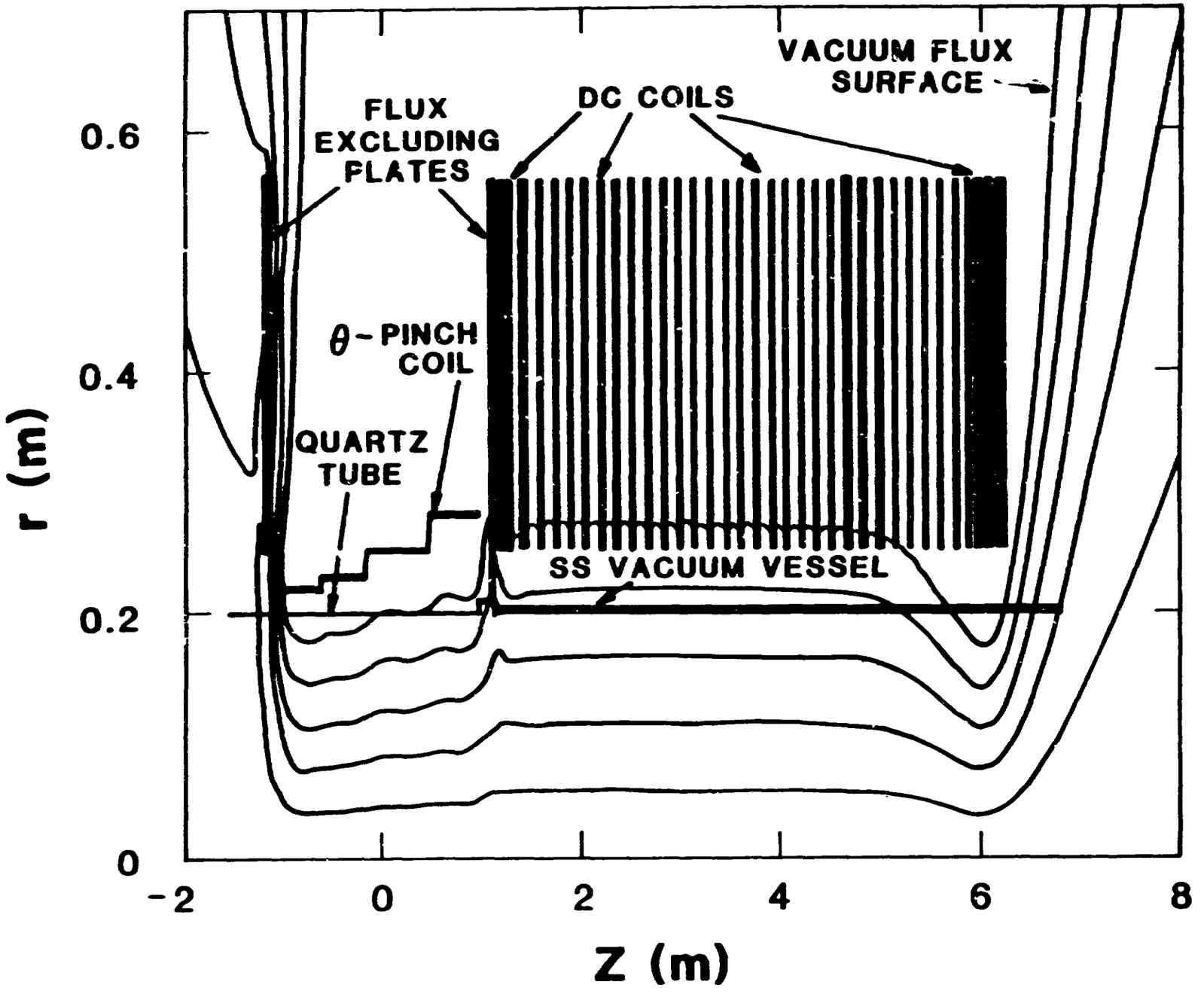
VACUUM FLUX
SURFACE
DC COILS
FLUX
EXCLUDING
PLATES
θ-PINCH
COIL
QUARTZ
TUBE
SS VACUUM VESSEL
r (m)
0.6
0.4
0.2
0
-2
0
2
4
6
8
Z (m)

B/84c1r547

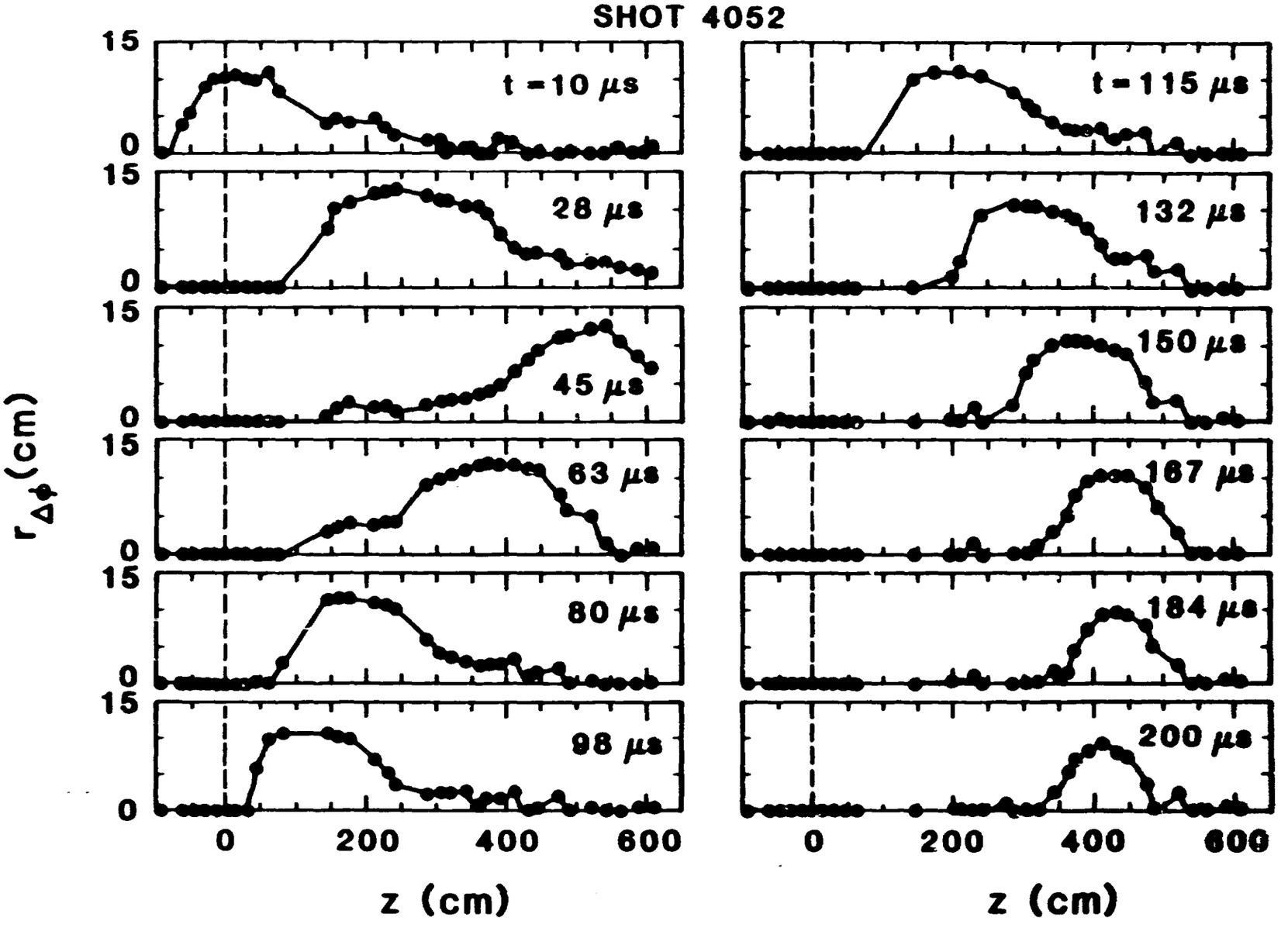
SHOT 4052
t = 10 μs
28 μs
45 μs
63 μs
80 μs
98 μs
t = 115 μs
132 μs
150 μs
167 μs
184 μs
200 μs
15
0
0
200
400
600
z (cm)
$r_{\Delta\phi}$ (cm)

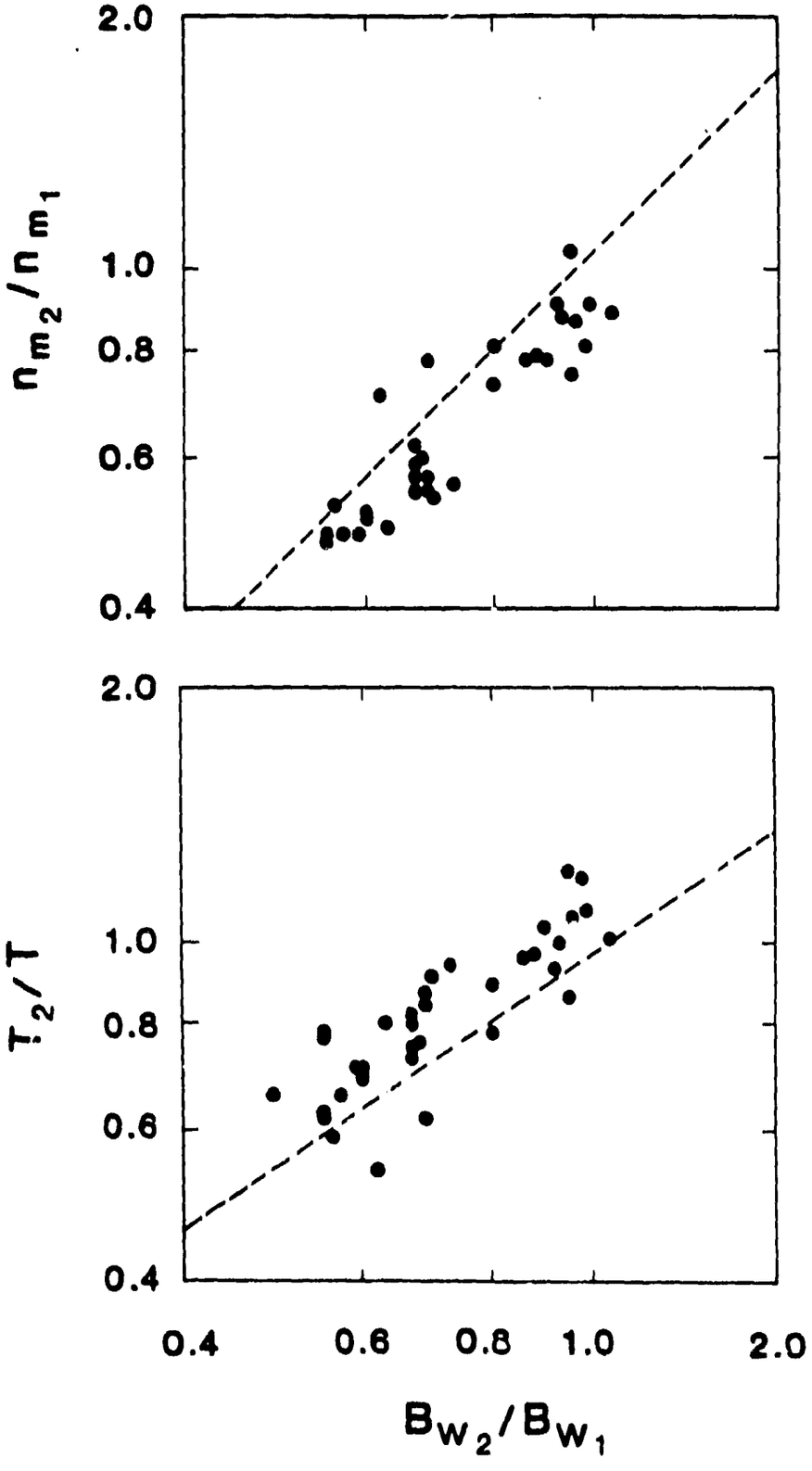

Fig. 20

3/84ctr6748

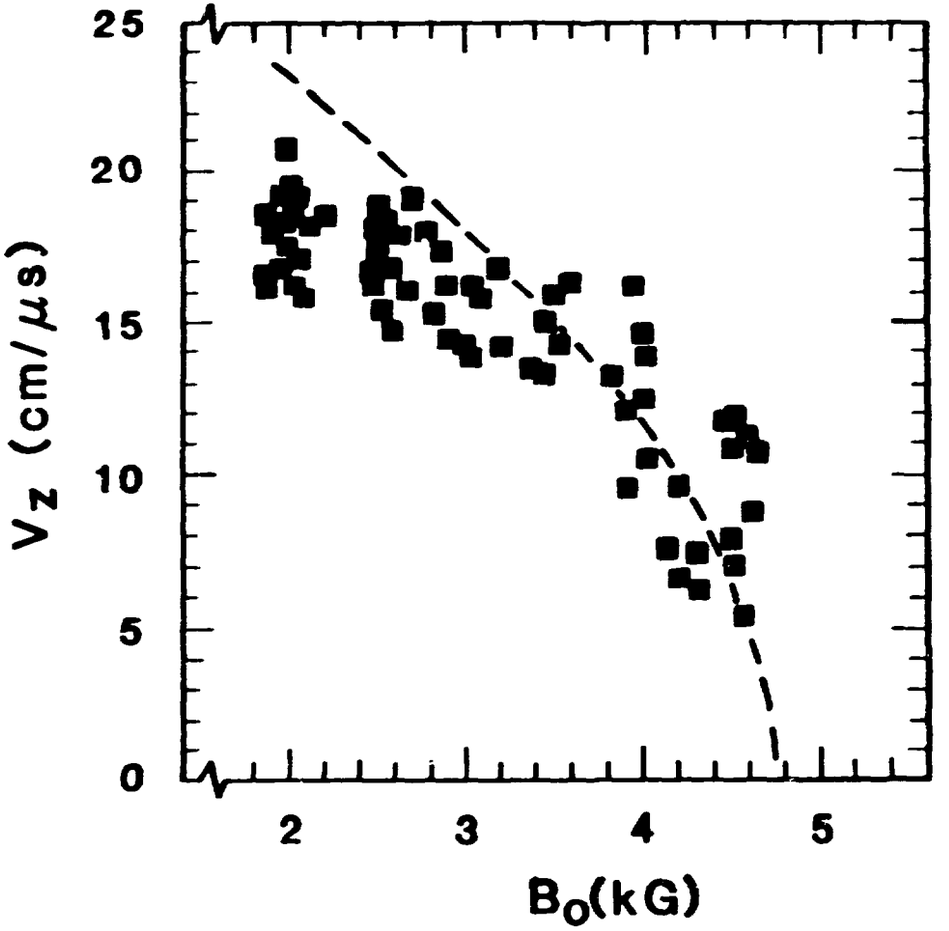
25
20
15
10
5
0
V_z (cm/μs)
2
3
4
5
B_0(kG)

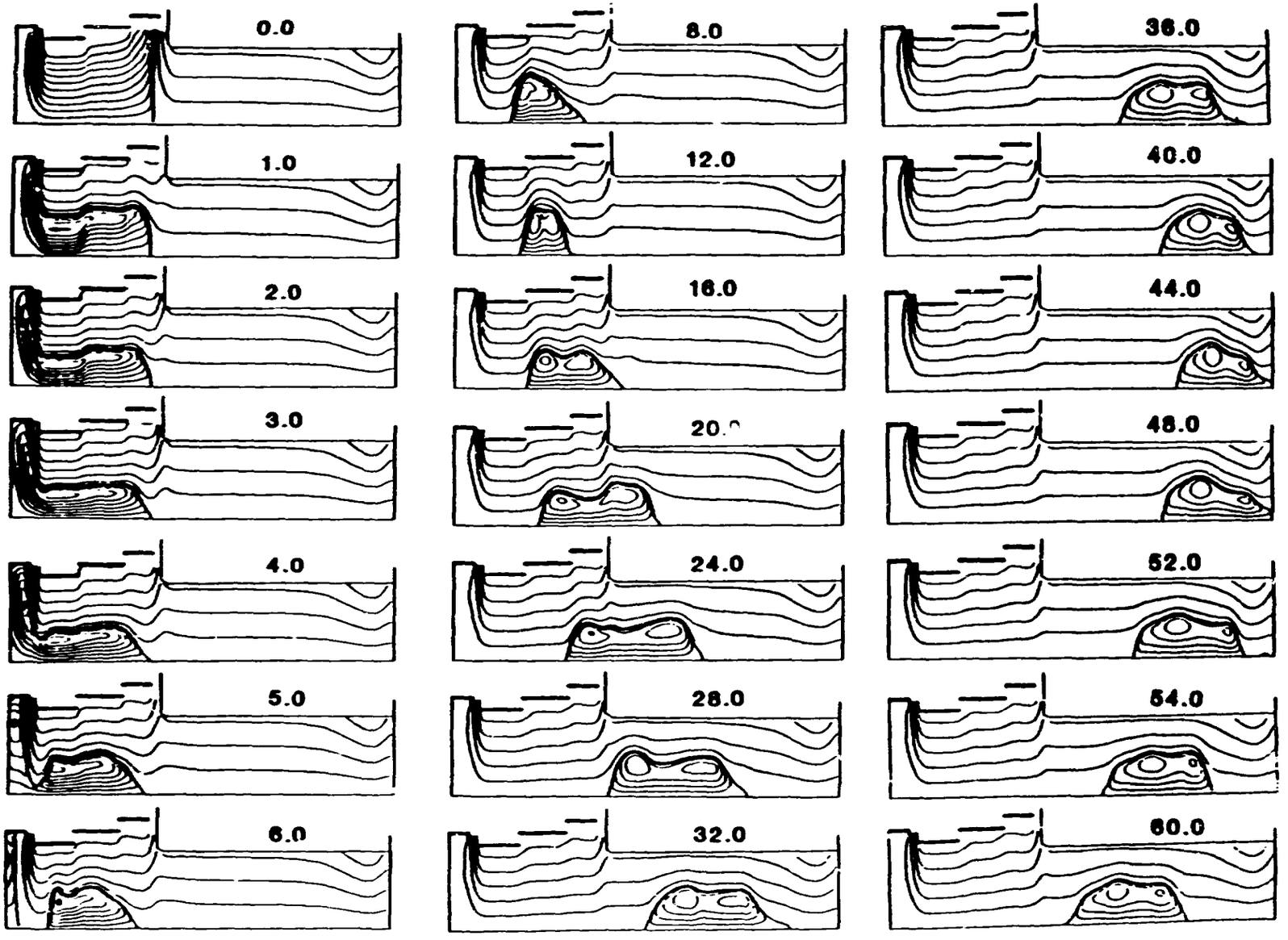
0.0
1.0
2.0
3.0
4.0
5.0
6.0
8.0
12.0
16.0
20.0
24.0
28.0
32.0
36.0
40.0
44.0
48.0
52.0
56.0
60.0

3/85ctr5749

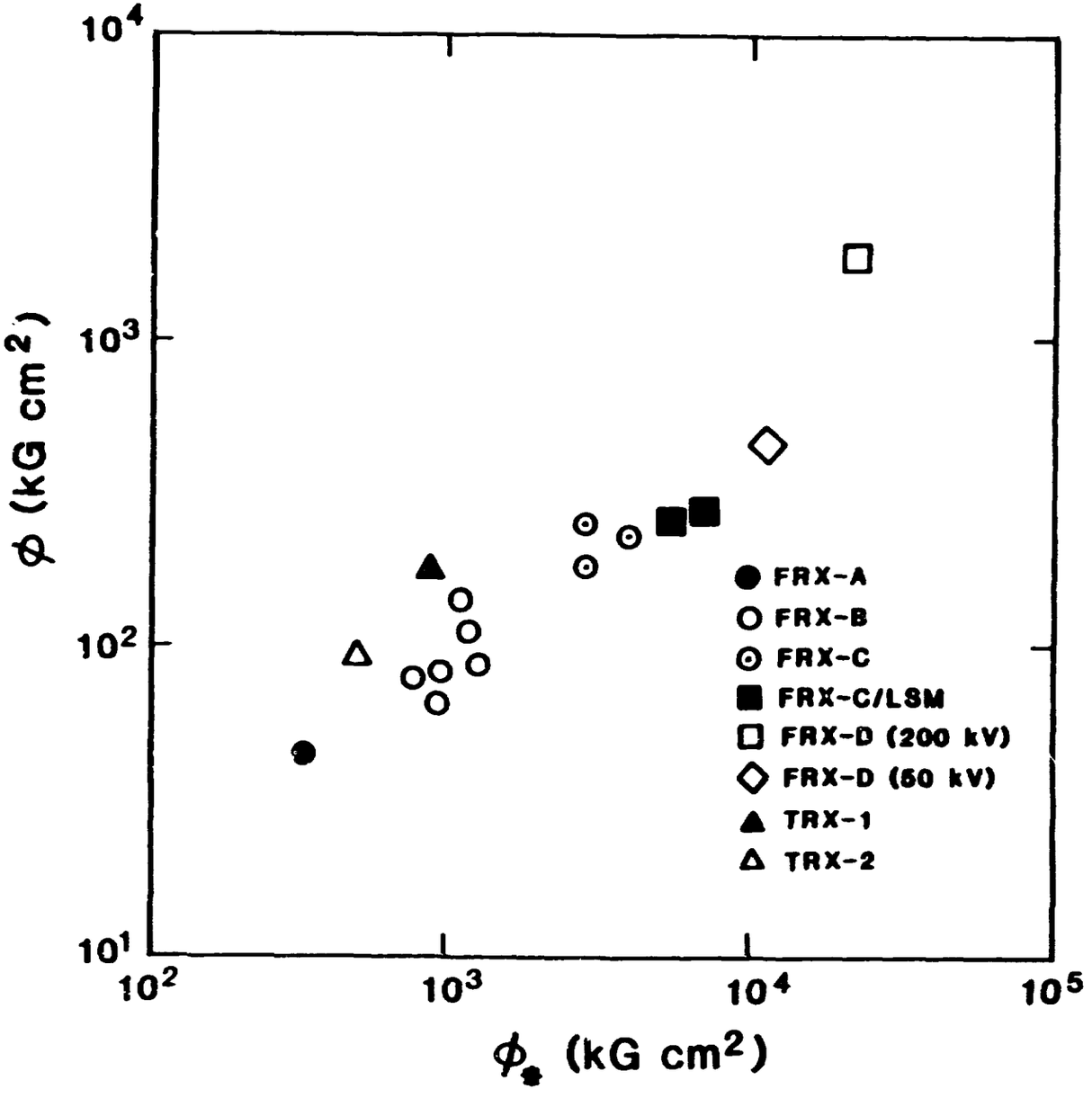
10^4
10^3
10^2
10^1
ϕ (kG cm^2)
10^2
10^3
10^4
10^5
ϕ_* (kG cm^2)
FRX-A
FRX-B
FRX-C
FRX-C/LSM
FRX-D (200 kV)
FRX-D (50 kV)
TRX-1
TRX-2

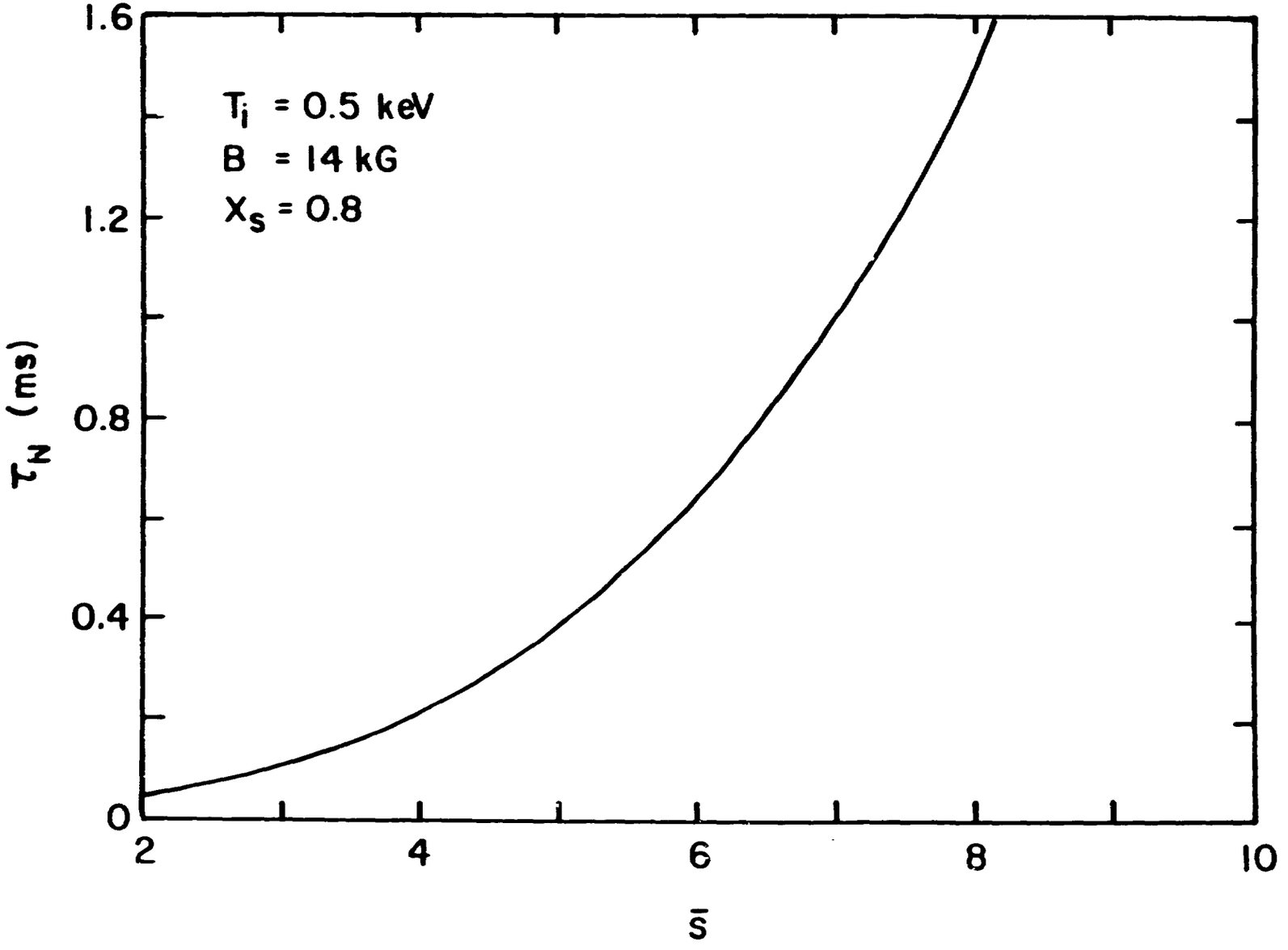

Fig. 24

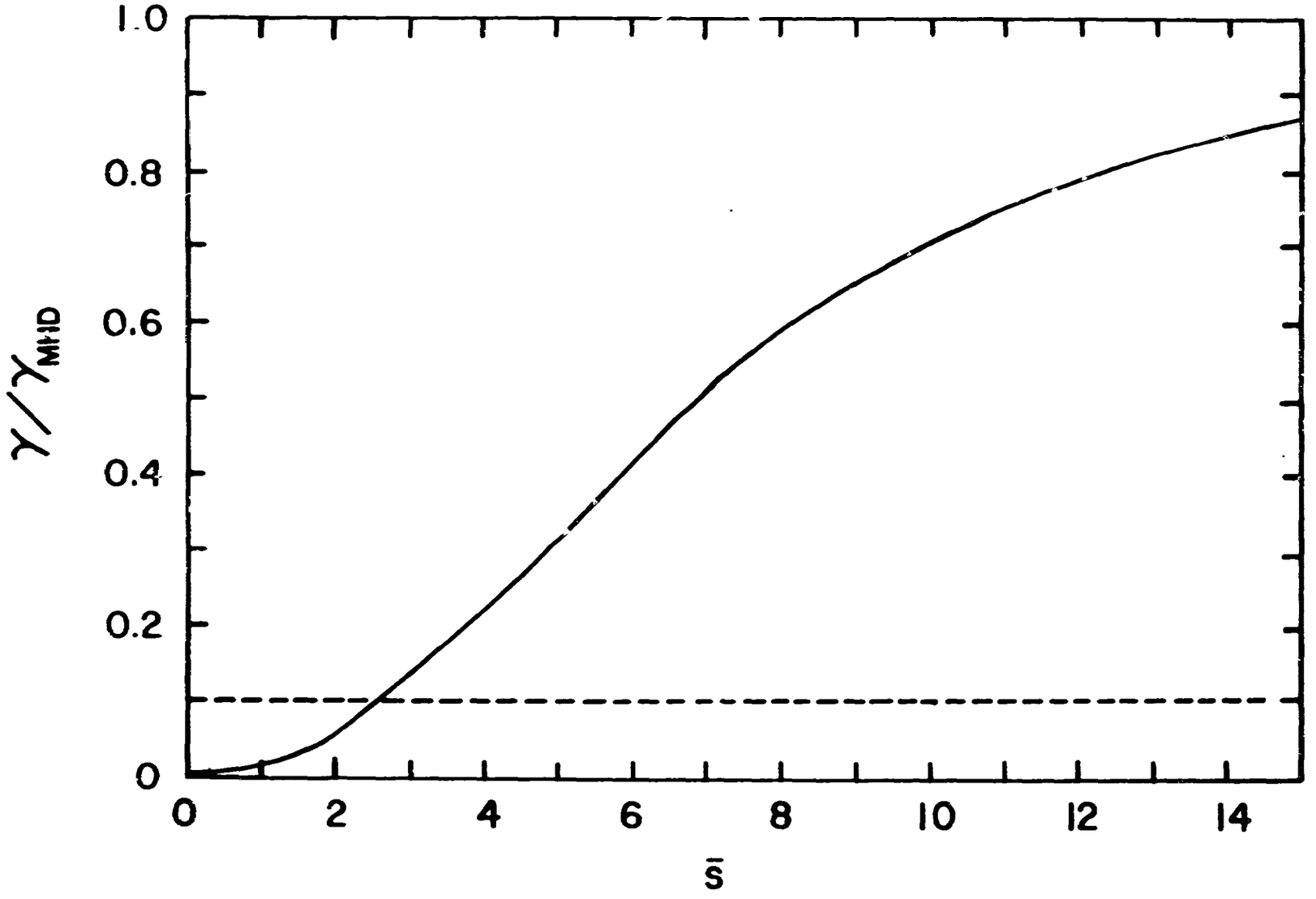

Fig. 22

FRX-D COIL SYSTEM